A Pictorial History of the Neuronal Cytoskeleton

Christophe Leterrier

JNeurosci
THE JOURNAL OF NEUROSCIENCE
January 6, 2021 • Volume 41 Number 1 • www.jneurosci.org

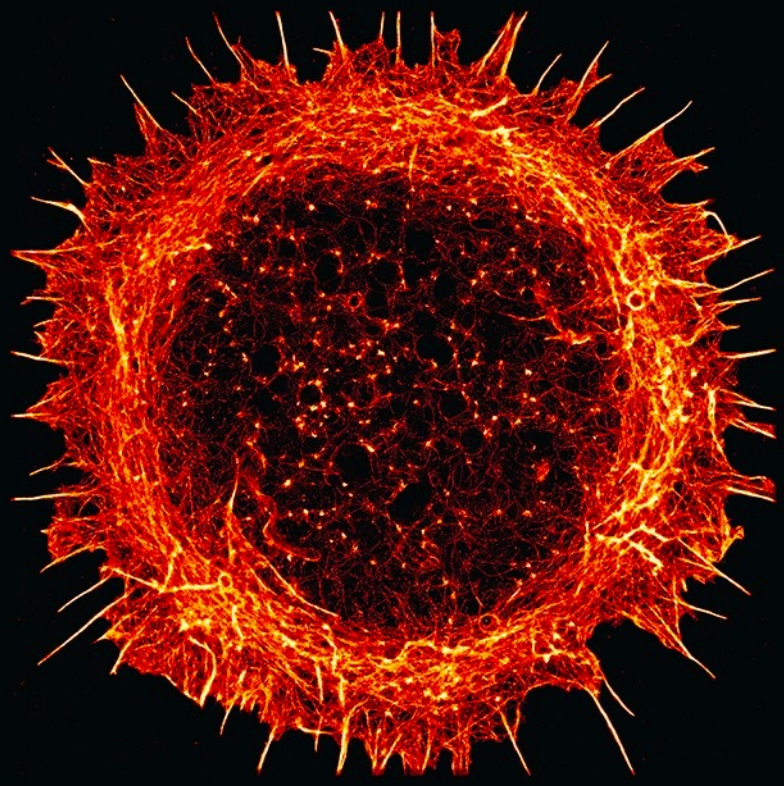

This Week in The Journal

- Amygdala Projections to Lateral Hypothalamus Elicit Avoidance
- The Protease Legumain Causes Oral Cancer Pain

SfN Society for Neuroscience

JN | Celebrating 40 years

Viewpoints

A Pictorial History of the Neuronal Cytoskeleton

Christophe Leterrier
Aix Marseille Université, Centre National de la Recherche Scientifique, INP Unité Mixte de Recherche 7051, NeuroCyto, Marseille 13005, France

Neurons are the "delicate and elegant...butterflies of the soul," as Santiago Ramón y Cajal famously put it in his memoir (Zwirn, 2015). Neurons interconnect throughout the brain and body via the elaborate arborization of their dendrites and axon. Their cytoskeleton, the intricate array of microtubules, intermediate filaments, and actin filaments running throughout each neuron, allows them to build, maintain, and transform their fantastic architectures (Leterrier et al., 2017; Tas and Kapitein, 2018). The 40th anniversary of the *Journal of Neuroscience* first issue marks a great occasion to showcase how images have shaped our understanding of the neuronal cytoskeleton, from the early drawing of pioneers to the latest developments of microscope technology. I will follow how preparation and culture procedures, staining methods, and microscopy techniques each brought new insight on key neuronal structures, such as microtubules, the axonal growth cone, and dendritic spines.

This history of the cytoskeleton in pictures begins in the 19th century with the drawings of gifted scientists/artists. Staining techniques, such as the Golgi method and its refinements, revealed not only the morphology of isolated neurons, but also the details of intraneuronal fibers, which were termed "neurofibrils." Beautiful drawings from light microscopy observations by Cajal and others depict these straight or wavy neurofibrils inside the cell body, dendrites, and axon of a variety of neurons (Fig. 1*A*,*B*, from Frixione, 2009). The advent of microphotography allowed images to be captured directly from the microscope, but drawings were still used throughout the 20th century to summarize findings as platonic ideals from numerous observations. Classic electron microscopy (EM) works from the 1950s to 1970s thus feature often beautiful, detailed drawings, such as the depiction of intermediate filament ("neurofilament") loops within presynapses from George Gray and Ray Guillery (Fig. 1*C*, from Gray and Guillery, 1966) or the summary of Victoria Chan-Palay's observations on the submembrane organization of the axon initial segment (Fig. 1*D*, from Chan-Palay, 1972). The abstraction offered by drawings makes them a natural choice to recapitulate current knowledge in textbooks, such as the works of art by Radivoj V. Krstić (Fig. 1*E*, from Krstić, 1979). Today's quantitative imaging has more rigorous and modern ways to refine and recapitulate information from a set of observations, but one may regret the artfulness and communication efficiency of these wonderful drawings, and hope for their renewed presence in scientific articles (Chabrier and Janke, 2017).

EM was instrumental in visualizing the details of cytoskeletal organization, with numerous ultrastructural studies in the 1940s and 1950s. The accuracy of EM observations goes hand in hand with the development of better fixation and sample processing techniques. Inclusion in plastic resin, then aldehyde fixation (Sabatini et al., 1963) greatly improved preservation of the neuronal cytoskeleton, allowing visualization of distinct microtubules; compare a typical osmic-acid fixed sample (Fig. 2*A*, from Horridge and Mackay, 1962) with a formaldehyde-fixed sample (Fig. 2*B*,*C*, from Sandborn et al., 1964). This opened the golden era of thin-section EM of the nervous system, with the ultrastructural definition of the three main cytoskeleton components: microtubules, intermediate filaments, and actin. Microtubules ("neurotubules") appear as hollow, 25-nm-diameter tubes running longitudinally along dendrites and axons (Prokop, 2020) in culture (Fig. 2*D*, from Bartlett and Banker, 1984) and *in vivo* (Fig. 2*E*, from Gonatas and Robbins, 1965). In cross-section, axonal microtubules appear as small rings, and along the axon initial segment, they can be seen closely linked together in characteristic bundles named "fascicles" (Fig. 2*F*, from Chan-Palay, 1972). Classic thin-section EM is still the method of choice for investigating nerve architecture, in particular in transverse sections of peripheral nerves, which show the arrangement of microtubules inside axons and the morphology of the myelin sheet surrounding them (Fig. 2*G*, from Katanov et al., 2020). Intermediate filaments ("neurofilaments") are thinner, 10 nm longitudinal filaments (Fig. 2*B*,*C*). Actin filaments ("microfilaments") are usually more difficult to discern on these images, appearing as a network of 7-nm-thick filaments at the periphery of axons, as well as within growth cones and filopodia ("microspikes," Fig. 2*H*, from Yamada et al., 1970).

Early on, microtubules were considered key components in establishing and maintaining neuronal architecture (Kapitein and Hoogenraad, 2015). Their role in transporting cellular components was suggested in the 1960s and strengthened by the observation of axonal microtubule bundles decorated with attached vesicles (Fig. 3*A*,*B*, from Smith et al., 1970; Smith, 1971). Refinements in EM sample preparation and imaging brought additional insight about microtubule organization in the 1980s and 1990s: painstaking serial reconstruction from multiple EM sections revealed the three-dimensional arrangement of microtubules along axons (Fig. 3*C*–*E*). The "hook" method, where microtubules are made to polymerize in a branched way using a specific buffer just before fixation, was able to resolve the orientation of microtubules (Fig. 3*F*, from

Received Nov. 13, 2020; revised Nov. 24, 2020; accepted Nov. 24, 2020.

I thank Marina Picciotto, Teresa Esch, and the *Journal of Neuroscience* staff for giving me the opportunity for this essay and for their assistance throughout its making; Marie-Jeanne Papandréou, Stéphane Vassilopoulos, and Subhojit Roy for insightful discussions and critical feedback; and Jean-Bernard Manent, Jean-Marc Goaillard, and Frédéric Chavane for helping me source classic *Journal of Neuroscience* covers.

The authors declare no competing financial interests.

*Correspondence should be addressed to Christophe Leterrier at christophe.leterrier@univ-amu.fr.

https://doi.org/10.1523/JNEUROSCI.2872-20.2020

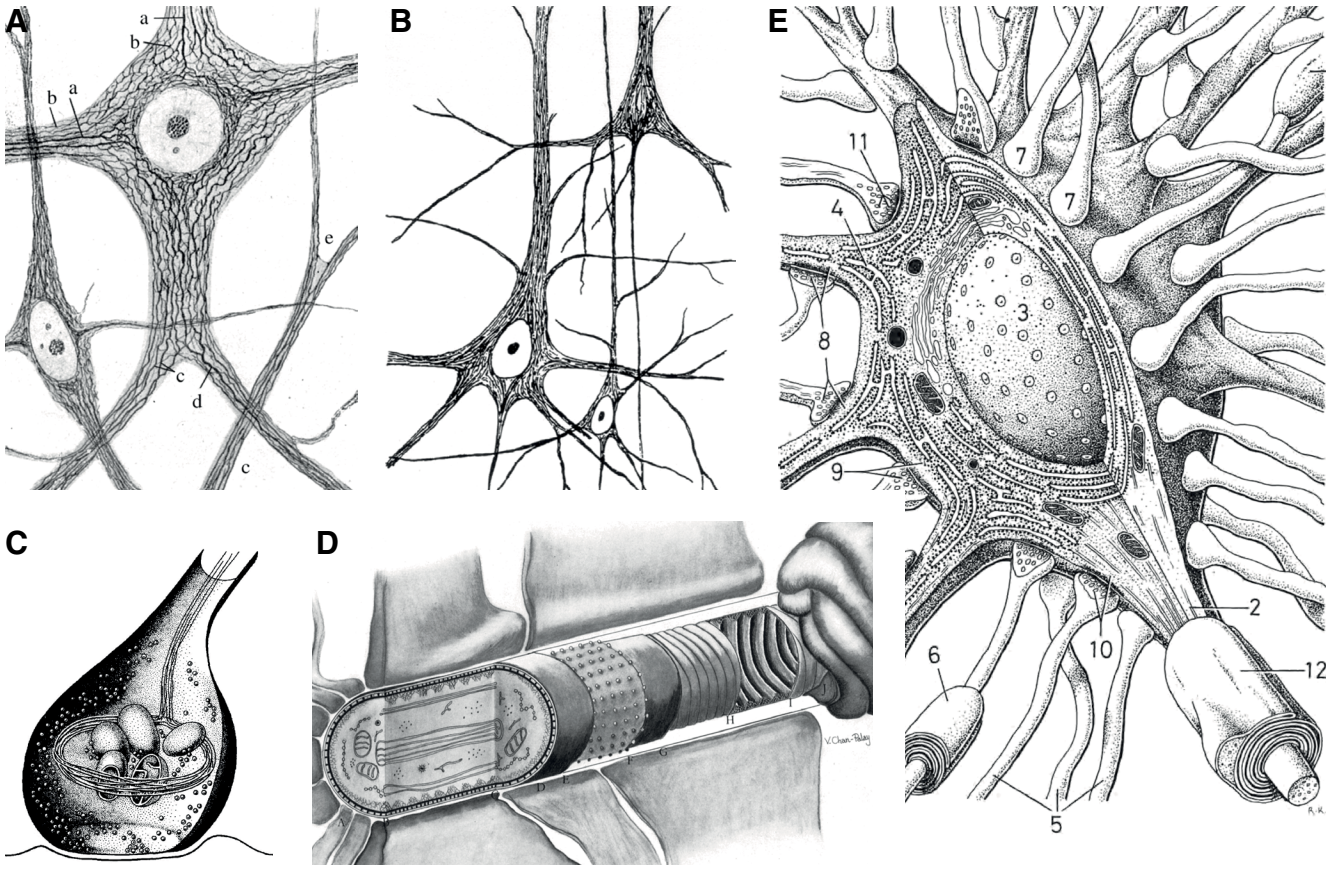

Figure 1. The neuronal cytoskeleton as drawn by scientists. ***A***, ***B***, Funicular cells of a young rabbit (***A***) and pyramidal cells of the visual cortex (***B***), as drawn by Cajal (1903). The reduced silver nitrate staining highlights neurofibrils inside the cell body and processes. Adapted from Frixione (2009). ***C***, Diagram of a spinal cord synapse showing a loop of neurofilaments, as seen by EM after osmium preparation. Adapted from Gray and Guillery (1966). ***D***, Drawing recapitulating the organization of the initial segment in Purkinje cells, with the microtubule bundles and the tripartite submembrane coat. Adapted from Chan-Palay (1972). ***E***, An archetypal neuron with its intracellular organization and synaptic contacts as drawn by Krstić (1979).

Baas et al., 1988) and showed that microtubules are uniformly plus-end distal in axons, but have a mixed orientation in dendrites (see also Figs. 7*B*, 8*B*, from Baas and Lin, 2011). Protofilaments within the microtubule lattice were visualized thanks to tannic acid fixation, which demonstrated, for example, the existence of unusual 15-protofilaments microtubules in touch neurons of the worm *Caenorhabditis elegans* (Fig. 3*G*, from Chalfie and Thomson, 1982). Immunogold labeling against tubulin post-translational modifications, indicative of microtubule age and stability, showed that different parts of axons have distinct modifications and stability profiles, and that the same microtubule can have segments bearing different modifications (Fig. 3*H*, from Baas et al., 1993). Twenty-five years later, progress in EM is still exciting, with cryo-EM promising another leap in our understanding of the neuronal cytoskeleton, by allowing visualization of macromolecular complexes *in situ* down to the near-atomic scale (Fig. 3*I*, from Atherton et al., 2018).

Beyond thin-section EM, alternative imaging modes have allowed unique ways to observe the neuronal cytoskeleton. Whole-mount transmission EM resolves the fine actin network within growth cones and filopodia (Fig. 4*A*,*B*, from Kuczmarski and Rosenbaum, 1979; Dailey and Bridgman, 1989). EM of platinum replicas, produced by rotary shadowing, beautifully reveals the inner network of the cytoskeleton after detergent extraction of the plasma membrane (Fig. 4*C*,*D*, from Letourneau, 1982; Stern et al., 2009). The quick-freeze, deep-etch technique, where the sample is rapidly frozen before being etched and replicated (Heuser, 2011), further revealed the intricate arrangement of cytoskeletal components within neurons (Fig. 5*A*, from Meller, 1987). This provided the stunning images obtained by Tom Reese and Nobutaka Hirokawa, showing the axon interior crowded with longitudinal microtubules and intermediate filaments, and interspersed with vesicles and organelles traveling along microtubules (Fig. 5*B*,*C*, from Hirokawa, 1982; Schnapp and Reese, 1982).

Immunolabeling with fluorescent antibodies for observation using light microscopy was invented in the 1940s (Coons et al., 1942) but was not used to image the neuronal cytoskeleton until much later, and then primarily in neuronal cultures. Antibodies against tubulin and actin (or fluorescent phalloidin) labeled microtubule and actin filaments in the processes of neuroblastoma cells (Fig. 6*A*, from Marchisio et al., 1978), revealing the organization of microtubules along neurites and the meshwork of actin within growth cones. The restriction of the microtubule-associated protein MAP2 to the somatodendritic compartment was first shown by comparison to tubulin immunolabeling (Fig. 6*B*, from Cáceres et al., 1986). By the end of the 1990s, fixation and staining protocols had been refined to their contemporary state, with fluorescent phalloidin, anti-tubulin, and MAP2 antibodies as standard labels (Fig. 6*C*, from Allison et al., 2000). Confocal microscopy, with its optical sectioning capabilities, was then used to generate 3D reconstructions of the neuronal cytoskeleton (Fig. 6*D*, from Gallo and Letourneau, 1998). Better microscopes and processing allowed refinement of fluorescence imaging of actin and microtubules in fixed neuron during the 21st century (Fig. 6*E*, from Ruthel and Hollenbeck, 2003; and

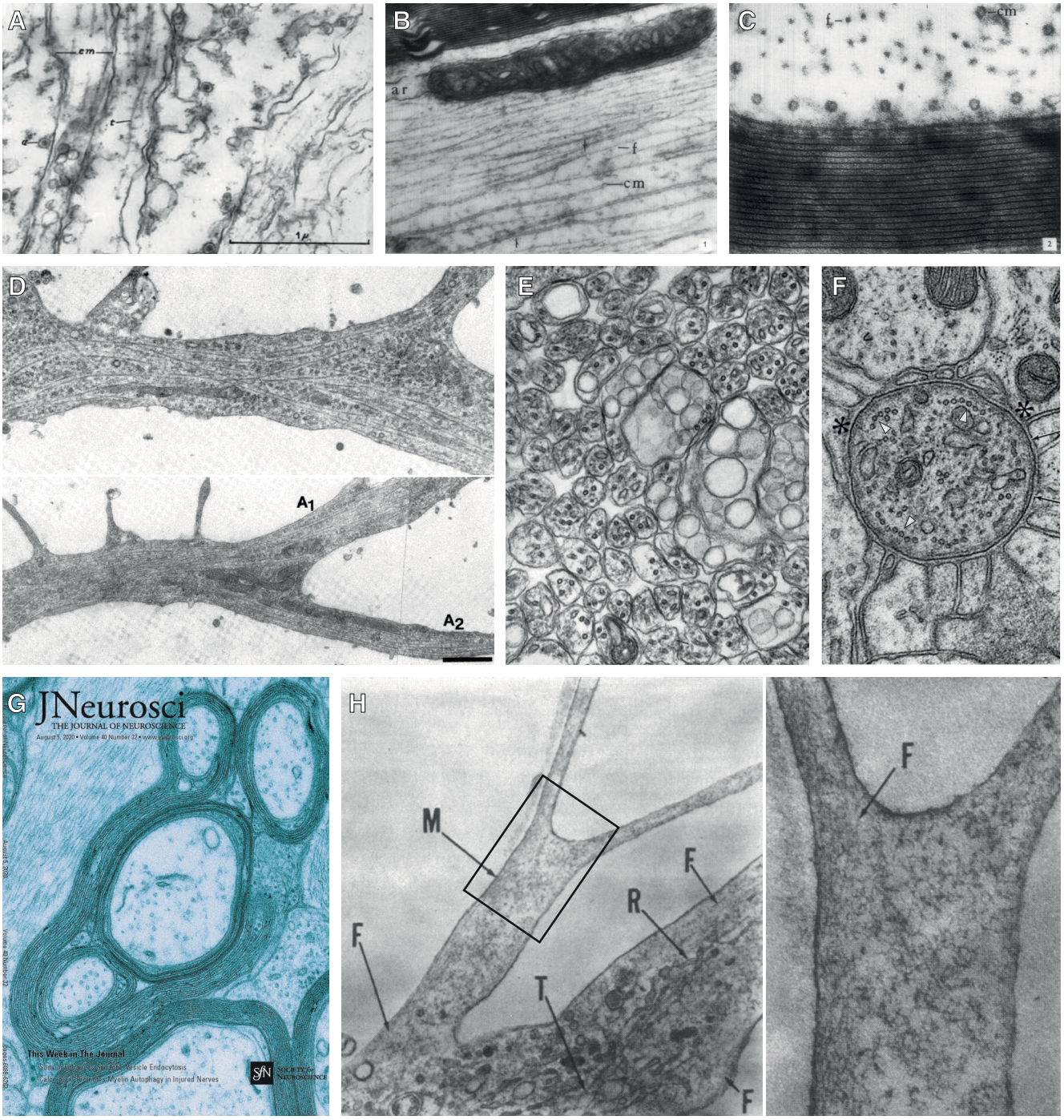

Figure 2. Classic electron microscopy (EM) images of the cytoskeleton inside neuronal processes. ***A***, Jellyfish axons fixed by osmic acid. A few neurotubules (t) are seen. Adapted from Horridge and Mackay (1962). ***B***, ***C***, The use of aldehydes for fixation led to better preservation of microtubules (cm) and neurofilaments (f), as seen in these longitudinal (***B***) and transverse (***C***) sections of myelinated axons from the semilunar ganglion of the rat. From these images, microtubules are measured as 22 nm in thickness (6 nm wall thickness, 10 nm lumen). Adapted from Sandborn et al. (1964). ***D***, EM image of cultured rat hippocampal neurons. Longitudinal sections along a dendrite (top) and the proximal axon (bottom, branches A1 and A2) from the same neuron. Tracks of microtubules are seen along the dendrite and axons, while polyribosomes are only present along the dendrite. Scale bar, 1.5 μm. Adapted from Bartlett and Banker (1984). ***E***, Axons from optic nerve fibers (embryonic chicken retina) in cross and diagonal sections showing microtubules as circular profiles, some of them containing intraluminal particles. Adapted from Gonatas and Robbins (1965). ***F***, Cross-section of a Purkinje cell axon initial segment showing connected fascicles of microtubules (arrowheads) and the undercoat lamina lining the inner side of the plasma membrane. Adapted from Chan-Palay (1972). ***G***, Cover from the August 5, 2020 issue of the *Journal of Neuroscience* showing a cross-section EM image of a sciatic nerve from a mouse lacking N-WASP in oligodendrocytes (Katanov et al., 2020). ***H***, Left, A filopodia (microspike [M]) from the axon of a DRG neuron, filled with a filamentous network (F) of actin. The main branch contains microtubules (T) and smooth endoplasmic reticulum (R). Right, Zoomed view. Adapted from Yamada et al. (1970).

Fig. 6*F*, distinguished at the 2017 Nikon Small World competition). Two key advances stand out: live-cell imaging to assess the dynamics of neuronal components, and super-resolution microscopy to resolve them at the nanoscale.

Dynamics are indeed a crucial aspect of the neuronal cytoskeleton and associated components: they underlie the morphologic changes that participate in synaptic plasticity and the evolution of neuronal shape over time. Before the broad adoption of live-cell

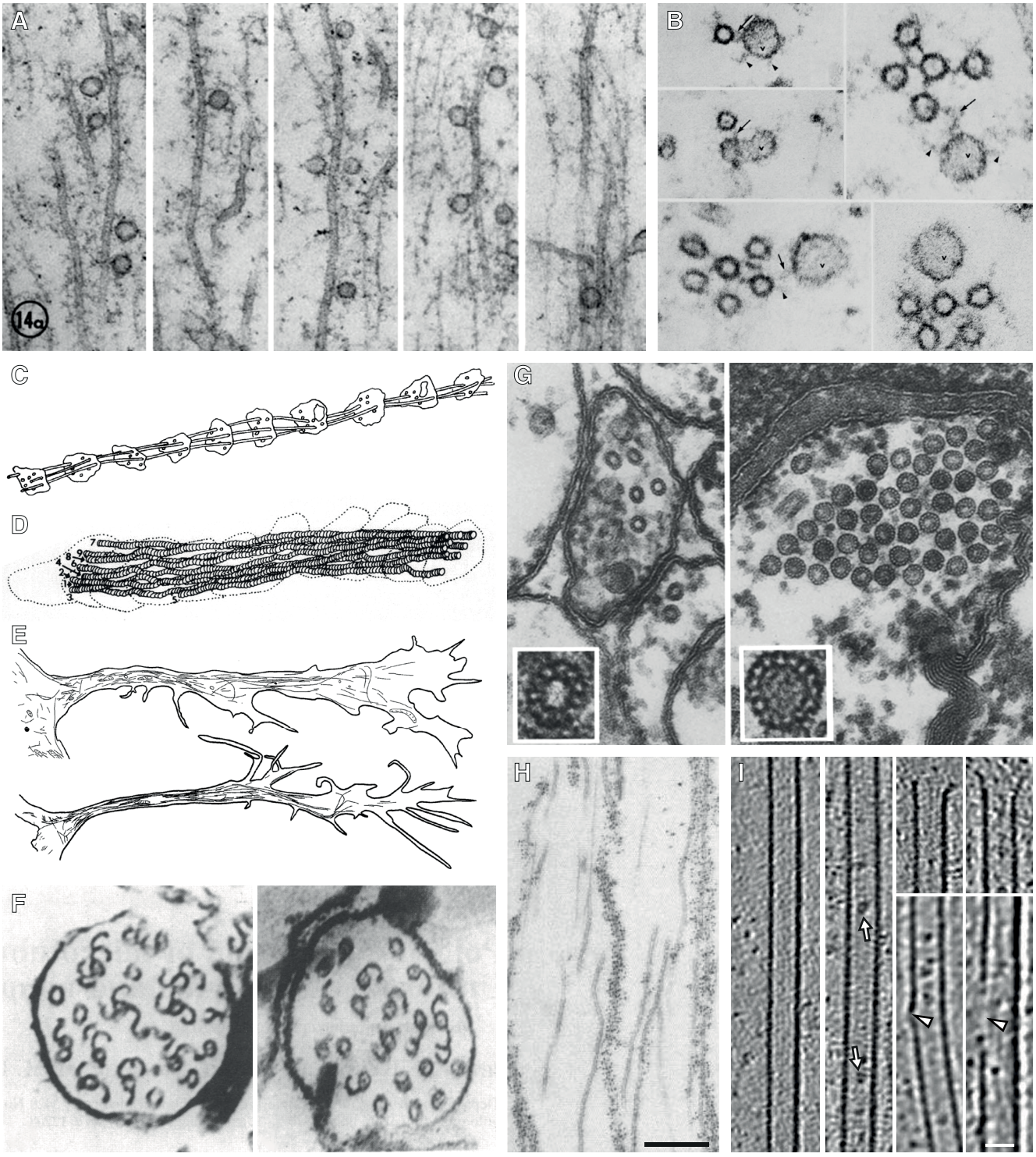

Figure 3. Refining the architecture of neuronal microtubules from EM images. ***A***, ***B***, Apposition of vesicles and microtubules suggesting their role in axonal transport. ***A***, Association of vesicular cargoes attached to microtubules along axons of the lamprey spinal cord. Adapted from Smith et al. (1970). ***B***, Corresponding transverse views showing bundles of connected microtubules and vesicles (v) along them with microtubule-vesicle links (arrows) and unattached projections (arrowheads). Adapted from Smith (1971). ***C–E***, Serial EM reconstructions used to reveal the 3D path of axonal microtubules. ***C***, Three microtubules traced over 6 μm along a rat sensory axon in organotypic culture of rat dorsal root ganglion neurons. Adapted from Bray and Bunge (1981). ***D***, Nine microtubules within an axon from chick optic tectum, traced over 10 μm. Adapted from Cheng and Reese (1988). ***E***, Drawing of microtubules along a single section from a serial section study of developing rat hippocampal neurons in culture, including a minor process of a neuron before axonal specification (top) and just after specification (bottom). The length of each neurite is ∼20 μm. Adapted from Yu et al. (1994). ***F***, Cross-section of axons from rat hippocampal neurons in culture prepared using the "hook" method. The direction of the hooks reveals that all microtubules have the same polarity, with their plus-ends directed toward the distal axon. Adapted from Baas et al. (1988). ***G***, Tannic acid fixation of *C. elegans* neurons reveals classic, 24-nm-diameter microtubules with 11 protofilaments (inset) in ventral cord neurons (left), whereas touch receptor cells contain larger, 30-nm-diameter microtubules with 15 protofilaments (right). Adapted from Chalfie and Thomson (1982). ***H***, Immunogold labeling of tyrosinated tubulin distinguishes tyrosinated (considered as labile) and detyrosinated (more stable) microtubules along the axon shaft of a rat sympathetic neuron in culture. Scale bar, 0.3 μm. Adapted from Baas et al. (1993). ***I***, Cryo-EM allows direct visualization of microtubules in cultured mouse neurons, revealing intraluminal particles (left, arrows), microtubule ends (top right), and defects along the lattice (bottom right, arrowheads). Scale bar, 20 nm. Adapted from Atherton et al. (2018).

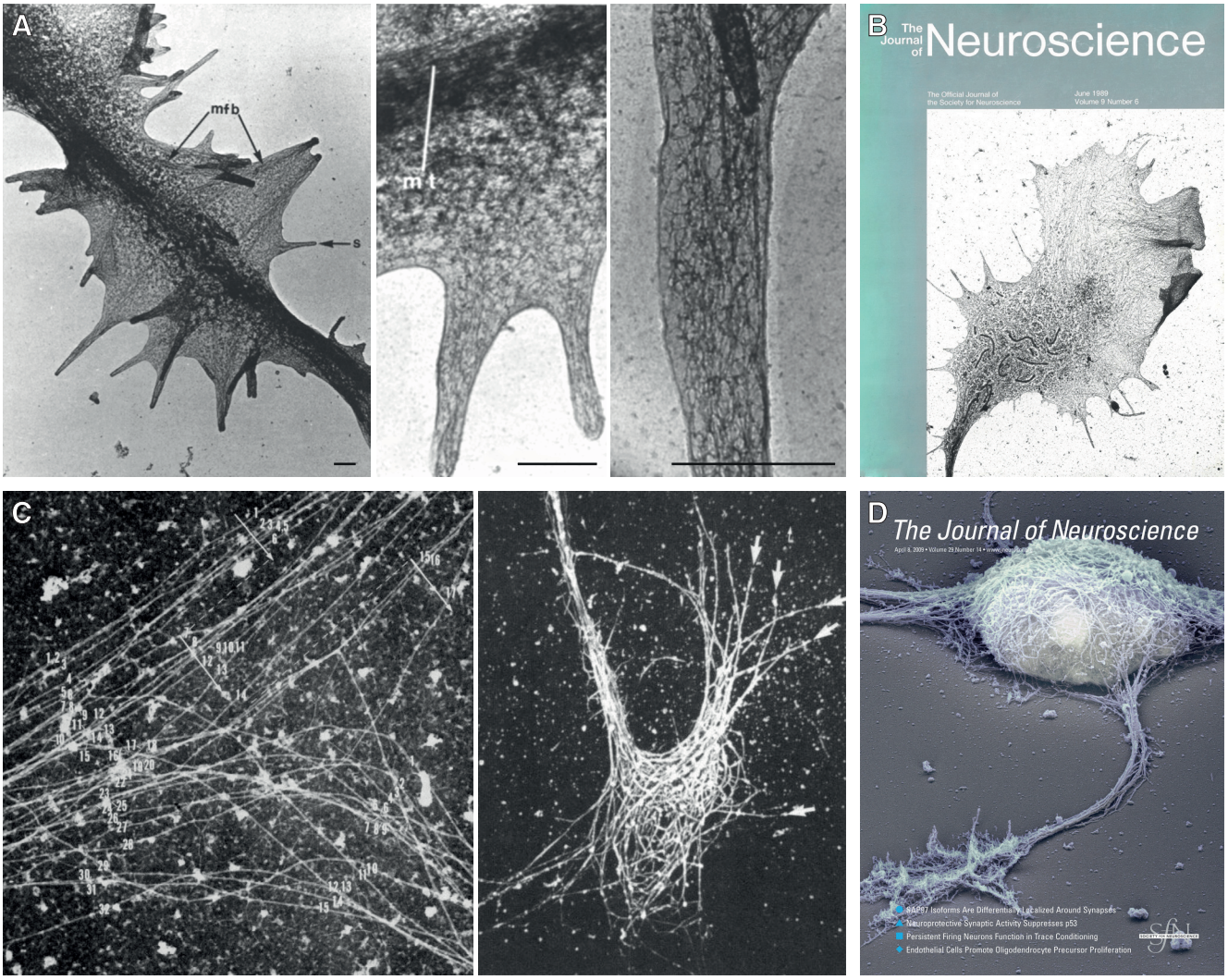

Figure 4. Different EM modalities reveal unseen views of the neuronal cytoskeleton. ***A***, Whole-mount transmission EM images of neuroblastoma cells show a neurite with numerous filopodia (microspikes, s) containing actin filaments bundles (mfb) (left). Actin filament bundles extend from central microtubules (mt) within filopodia (center), where the actin network appears wavy (right). Scale bars, 0.5 μm. Adapted from Kuczmarski and Rosenbaum (1979). ***B***, Cover from the June 1, 1989 issue of the *Journal of Neuroscience* showing a whole-mount EM image of a growth cone (Dailey and Bridgman, 1989). ***C***, Transmission (left) and scanning (right) EM of extracted, shadowed cytoskeleton showing the organization of microtubules within the axon shaft (left) and in a growth cone (right) of chick sensory ganglia explants in culture. Adapted from Letourneau (1982). ***D***, Cover from the April 8, 2009 issue of the *Journal of Neuroscience* showing an extracted, rotary shadowed hippocampal neuron in culture (Stern et al., 2009).

imaging in the 2000s, investigation of cytoskeletal dynamics relied on ingenious endpoint experiments after time-controlled manipulation, such as injection of labeled tubulin to distinguish newly assembled and stable microtubules within neurons (Fig. 7*A*, from Slaughter et al., 1997). Live-cell imaging of microtubule plus-end associated proteins, such as EB1/EB3, complemented the hook approach to determine the orientation of growing microtubules along the axon and dendrites (Stepanova et al., 2003), an approach recently extended from cell culture to organotypic slices and living animals (Fig. 7*B*, from Yau et al., 2016). The diffusion of proteins and lipids along the plasma membrane is another important phenomenon for neuronal physiology; and the cytoskeleton, in particular the submembrane actin and scaffold, plays an important role in this movement (Kusumi et al., 2005). Measuring diffusion of lipids requires high-speed tracking of single particles; such experiments revealed a diffusion barrier at the axon initial segment (Fig. 7*C*, from Nakada et al., 2003; see also Fig. 13*C*). The diffusion of receptors in and out synapses is key to synaptic plasticity and learning (Groc and Choquet, 2020); single-particle tracking (SPT) of quantum-dot-labeled synaptic receptors allows researchers to dissect the mechanisms regulating their enrichment at the postsynapse (Fig. 7*D*, from Charrier et al., 2006). Nowadays, live-cell imaging continues to progress toward better temporal and spatial resolution, but also smarter schemes allowing the capture of rare events over long-term acquisitions.

The other major advance for neuronal cytoskeleton imaging was the development of super-resolution microscopy, a set of techniques able to bypass the ~250 nm diffraction limit of optical microscopy (Jacquemet et al., 2020). These techniques include single-molecule localization microscopy (SMLM), a method using sequential localization of individual fluorescent emitters and comprising techniques, such as stochastic optical reconstruction microscopy (STORM), photo-activation localization microscopy (PALM), and DNA point accumulation in nanoscale topography (PAINT); structured illumination microscopy (SIM), which retrieves details beyond the diffraction limit using the moiré produced by patterned illumination of the sample; stimulated emission depletion microscopy (STED), a point-

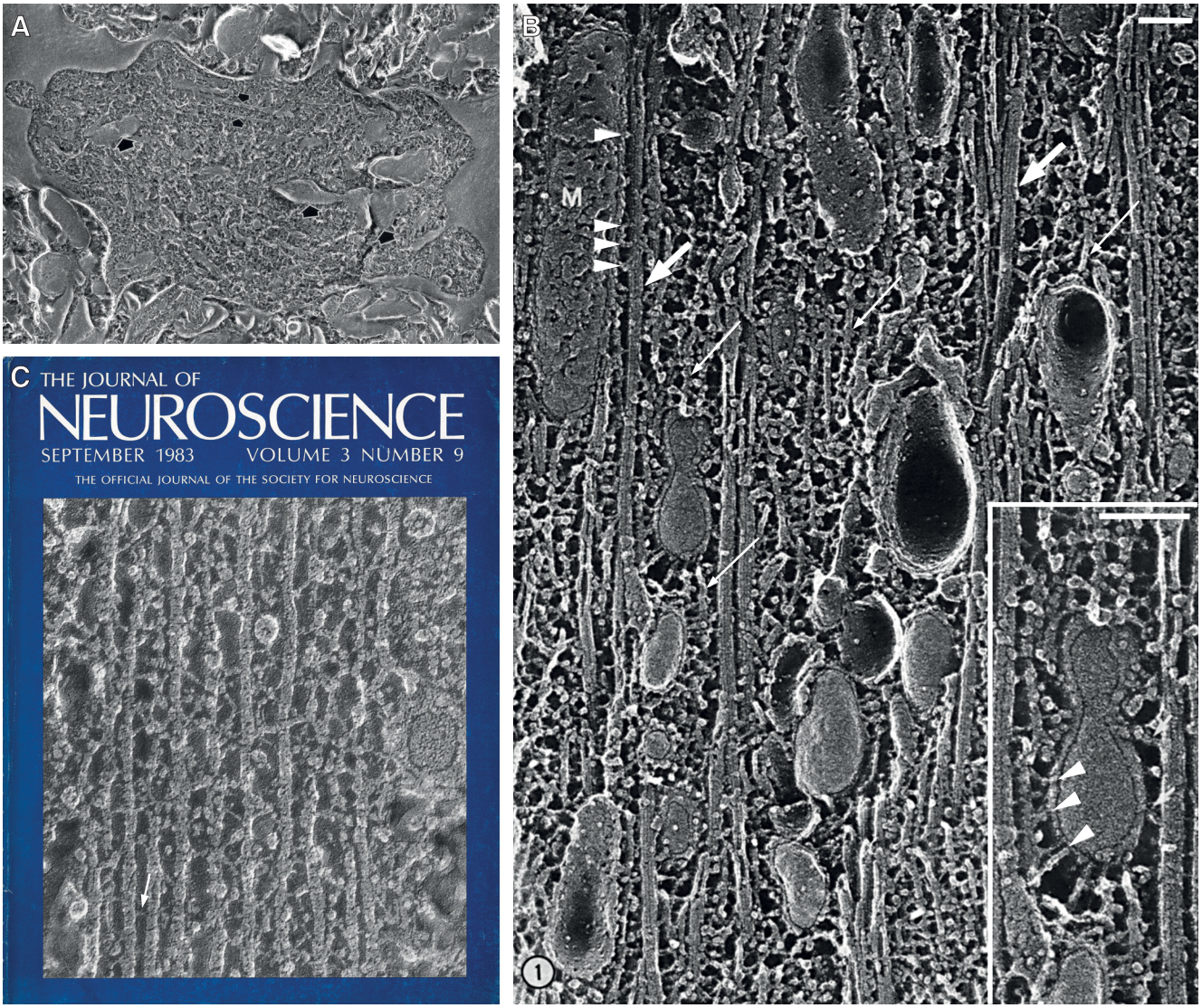

Figure 5. Freeze etching reveals the neuronal cytoskeleton at the macromolecular scale. ***A***, Cryo-fixed, freeze-etched dendrite from a chicken Purkinje cell. The open dendrite reveals intracellular organelles (large arrows) and microtubules (small arrows) embedded in a dense meshwork. Adapted from Meller (1987). ***B***, The technique of quick-freeze, deep etching can reveal the cytoskeleton with unprecedented details. In this axon from frog spinal cord, one can see numerous microtubules (arrows) cross-linked with neurofilaments (small arrows), and vesicular cargoes as well as mitochondria (M) often connected to microtubules by linker proteins (arrowheads). Scale bars, 0.1 μm. Adapted from Hirokawa (1982). ***C***, Cover from the September 1, 1983 issue of the *Journal of Neuroscience* showing a similar quick freeze, deep-etch preparation from turtle optic nerves (Schnapp and Reese, 1982).

scanning technique that reduces the size of the excitation point by superimposing a donut-shaped depletion beam; and expansion microscopy, a technique based on physical expansion of the sample using hydrogel swelling. Microtubules are densely packed in neuronal processes, and only refinements of SMLM using small nanobodies are able to resolve individual microtubules in axonal and dendritic bundles (Fig. 8*A*, from Mikhaylova et al., 2015). An elegant development merging PAINT and SPT is Motor-PAINT, which tracks recombinant motor proteins along the microtubules of fixed and extracted neurons, allowing examination of their nanoscale architecture and orientation (Fig. 8*B*, from Tas et al., 2017). Expansion microscopy is also a promising development for imaging microtubules, as it allows three-dimensional, multicolor imaging of tightly packed bundles inside dendrites using confocal imaging after sample expansion (Fig. 8*C*, from Jurriens et al., 2020). STED allows straightforward multicolor imaging, which recently revealed the interplay of actin patches, microtubules, and lysosomes along the dendritic shaft (Fig. 8*D*, from van Bommel et al., 2019). Finally, STORM attains a ~20 nm resolution, resolving the finest details of the actin cytoskeleton, such as spines bearing synapses in mature neurons (Fig. 8*E*) or actin hotpsots and filamentous trails within axons (Fig. 8*F*, from Ganguly et al., 2015).

Having presented the historical evolution of the different techniques, with a majority of examples showing neuronal microtubules, I would like to focus on how these techniques shaped our knowledge of two key actin-rich compartments: the axonal growth cone and dendritic spines. Growth cones, as drawn by Cajal in 1899 (Fig. 9*A*, from Cajal, 1999), are fan-shaped extremities of axons that sense the environment to drive axonal growth and pathfinding (McCormick and Gupton, 2020). Fluorescence imaging reveals how microtubules loop into the growth cone center, while actin shapes the peripheral, dynamic filopodia (Fig. 9*B*, from Biswas and Kalil, 2018). Live-cell imaging, first using injected tubulin and phalloidin to visualize microtubules and actin (Fig. 9*C*, from Dent and Kalil,

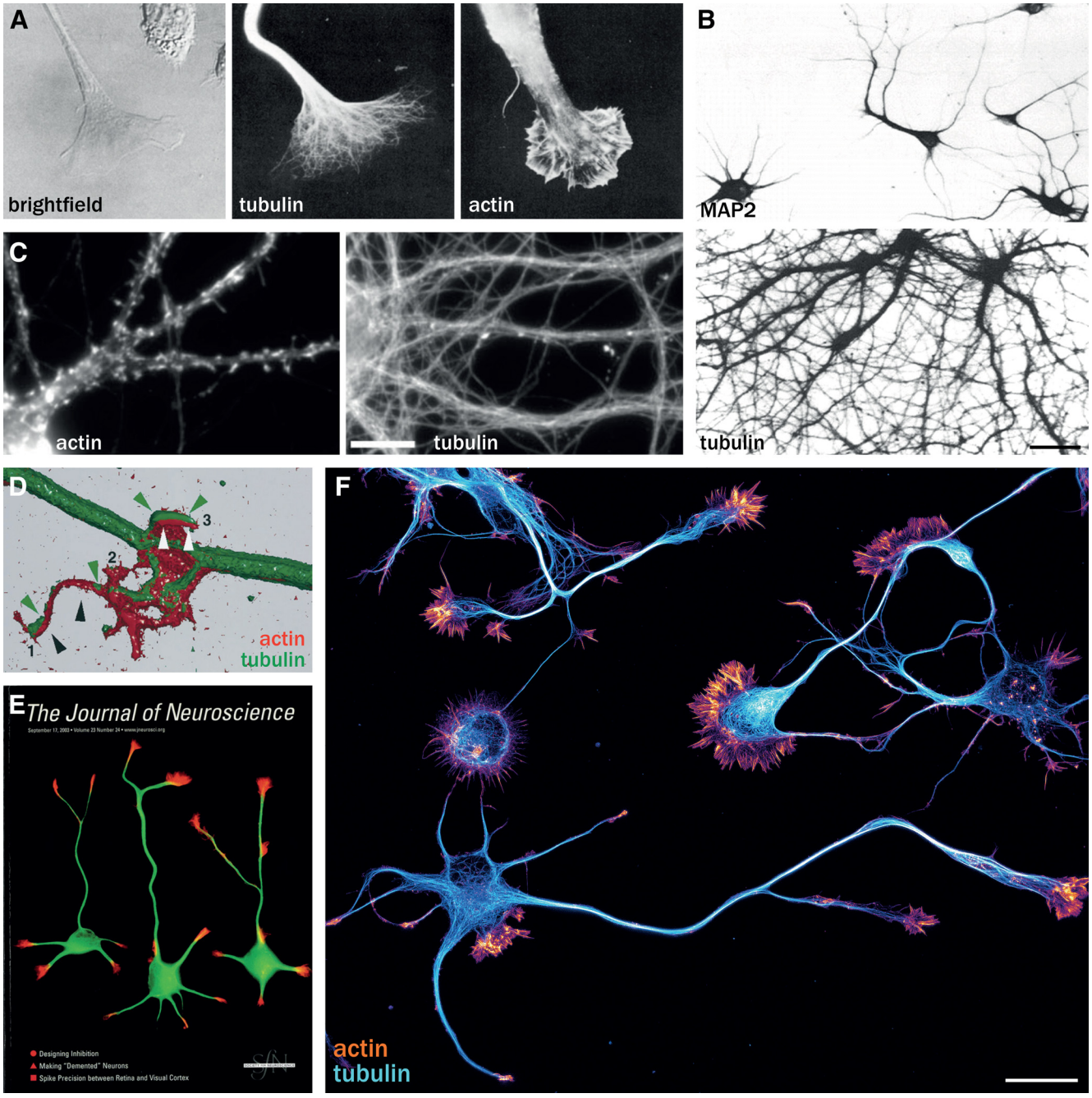

Figure 6. Using immunolabeling to visualize the neuronal cytoskeleton. ***A***, Three mouse neuroblastoma cells seen by brightfield (left), immunostained for tubulin (middle), and for actin (right). Adapted from Marchisio et al. (1978). ***B***, Immunolabeling for microtubule-associated protein MAP2 (left, segregated in the cell body and dendrites) and microtubules (right, present throughout the neuron) in different rat hippocampal neurons in culture. Scale bar, 50 μm. Adapted from Caceres et al. (1986). ***C***, Optimized labeling for actin (using fluorescent phalloidin, left) and microtubules (using anti-tubulin antibodies, right). Scale bar, 10 μm. Adapted from Allison et al. (2000). ***D***, Confocal microscopy of actin (red) and microtubules (green) allows for 3D reconstruction of the site of contact between a chick embryo dorsal root ganglia neuron in culture and two nerve growth factor-coated beads (not visible), with filopodia (1-3 numbers and arrowheads) contacting the beads. Adapted from Gallo and Letourneau (1998). ***E***. Cover from the September 17, 2003 issue of the *Journal of Neuroscience* showing developing rat hippocampal neurons in culture labeled for actin (red), concentrated at growth cones, and microtubules (green) present in the cell body and along neurites (Ruthel and Hollenbeck, 2003). ***F***, Rat hippocampal neurons after 2 d culture labeled for microtubules (cyan) and actin (orange). Scale bar, 20 μm. Unpublished image from the author.

2001) and later using fluorescent protein probes and sometimes super-resolution microscopy (Fig. 9*D*, from Fiolka et al., 2012), revealed the intricate rearrangement that drives growth cone twists and turns. Platinum replica EM of extracted growth cone provided stunning images of the dense, branched actin meshwork at the growth cone periphery (Fig. 9*E*, from Korobova and Svitkina, 2008) and its connections to central microtubules (Fig. 9*F*, from Burnette et al., 2008). SIM of actin at growth cones (Fig. 9*G*, from Igarashi et al., 2018) can be performed on living cells, revealing the interplay between endocytosis, vesicular trafficking, and actin organization (Fig. 9*H*, from Nozumi et al., 2017). More recent work has imaged growth cones in a 3D, soft collagen matrix using live-cell and STED microscopy, which showed some key architectural differences with the classically studied 2D situation of cells growing on glass (Fig. 9*I*, from Santos et al., 2020).

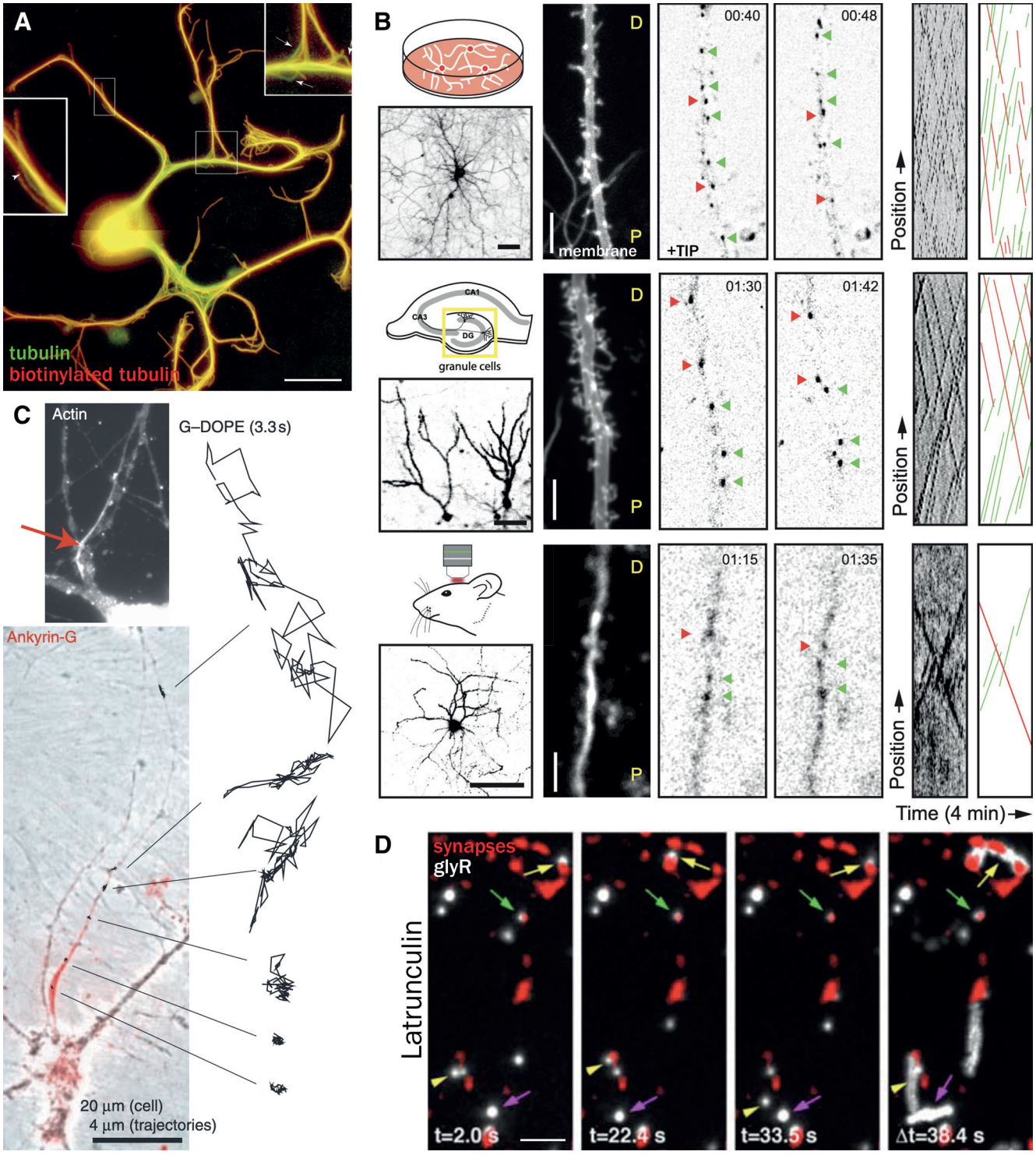

Figure 7. Live-cell imaging reveals the dynamics of the cytoskeleton and the neuron surface. ***A***, Sympathetic neuron in culture injected with biotinylated tubulin and fixed after 1.25 h of incubation. Microtubules that have turned over during incubation are positive for both tubulin (green) and biotinylated tubulin (red), whereas stable microtubules appear green, as seen along the growing axon (insets, arrows). Scale bar, 20 μm. Adapted from Slaughter et al. (1997). ***B***, Imaging of growing microtubules' plus-ends in living neurons from hippocampal cultures (top row), organotypic slices (middle row), and *in vivo* (bottom row). In each condition, comets are seen to move in both the proximal (P) and distal (D) directions along dendrites, demonstrating the bidirectional orientation of assembling microtubules (kymographs, right panels). Scale bars, 20 μm (in low-magnification images, left columns) and 5 μm (in dendritic segment images). Adapted from Yau et al. (2016). ***C***, High-speed measurements of G-DOPE lipid diffusion along the proximal axon. Trajectories (right) show immobilization of lipids along the initial segment (ankyrin G staining, red on bottom panel; actin staining, top panel) compared with the distal axon, demonstrating the existence of a diffusion barrier at the axon initial segment. Adapted from Nakada et al. (2003). ***D***, Diffusion of quantum-dot-labeled glycine receptors along the dendrites of spinal cord neurons. In control neurons and after actin disassembly by latrunculin, glycine receptors are more mobile outside of synapses (yellow and purple arrows). Last panel, Temporal projection (presynapses labeled with FM4-64). Scale bar, 5 μm. Adapted from Charrier et al. (2006).

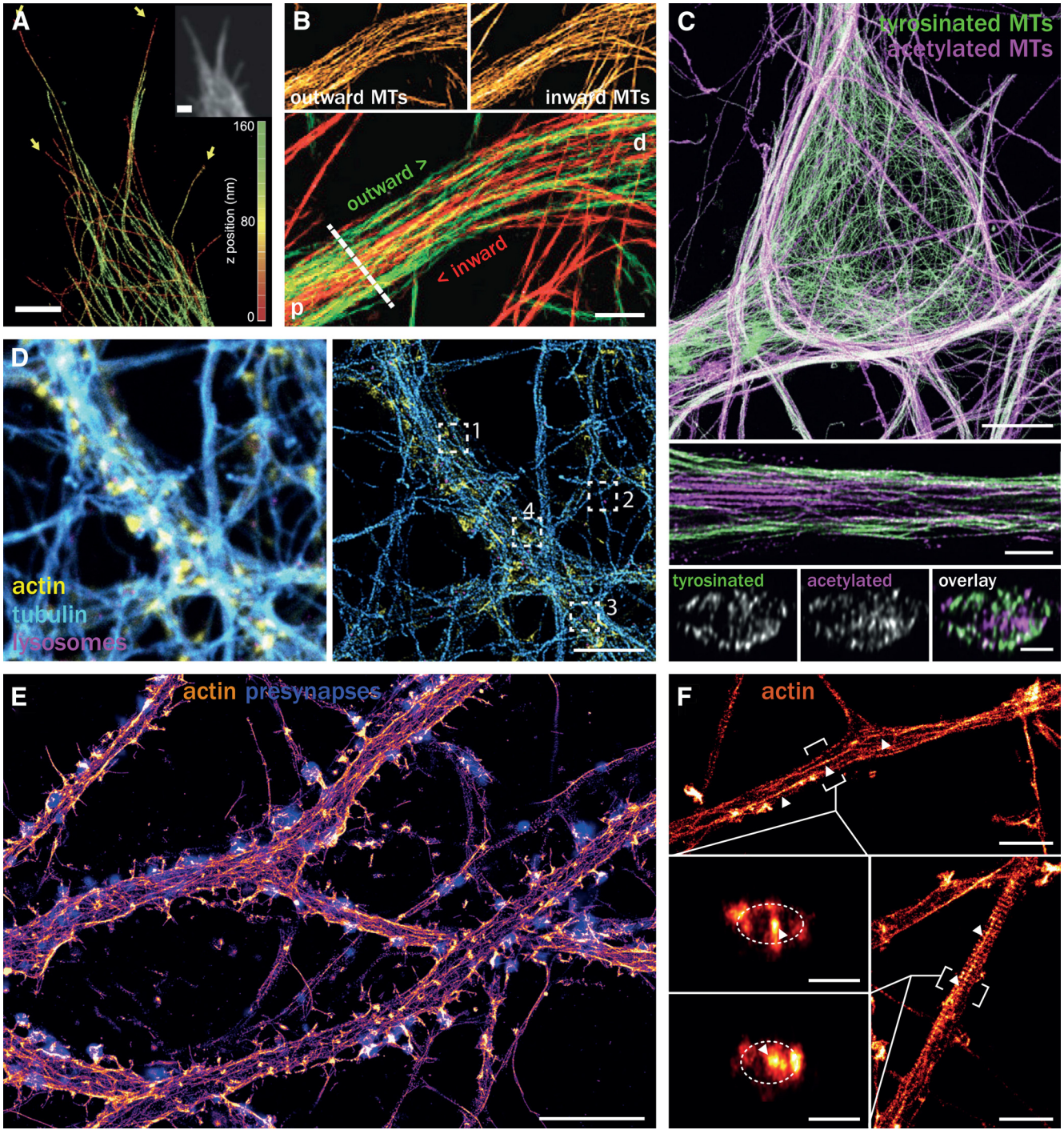

Figure 8. Nanoscale architecture of the neuronal cytoskeleton by super-resolution microscopy. ***A***, Nanobodies against tubulin allow labeling of densely packed microtubules inside rat hippocampal neurons in culture, as imaged by 3D-Stochastic Optical Reconstruction Microscopy (STORM). Scale bar, 2 μm. Adapted from Mikhaylova et al. (2015). ***B***, Motor-Point Accumulation in Nanoscale Topography (PAINT) can determine both the nanoscale organization and orientation of microtubules. It reveals the mixed orientation of dendritic microtubules, with outward-directed ones at the periphery (green on overlay) and inward-directed ones found deeper in the center of the dendrite (red on overlay). Scale bar, 1 μm. Adapted from Tas et al. (2017). ***C***, Expansion microscopy provides an ~5× enhancement in resolution over that delivered by the microscope (here confocal), detailing the organization of tyrosinated and acetylated (stabilized) microtubules, with acetylated microtubules found at the center of large dendrites (bottom panels, cross-sections). Scale bars: Top, 5 μm; Middle, Bottom, 2 μm. Adapted from Jurriens et al. (2020). ***D***, STimulation-Emission Depletion (STED) microscopy (right) shows enhanced resolution compared with confocal (left) in these views of hippocampal neurons labeled for actin (yellow), microtubules (cyan), and lysosomes (LAMP1, magenta). Scale bar, 5 μm. Adapted from van Bommel et al. (2019). ***E***, STORM imaging of actin in mature rat hippocampal neurons, with presynapses (synapsin) labeled in blue. Scale bar, 5 μm. Unpublished image from the author. ***F***, 3D-STORM of actin along axons reveals the presence of clusters (actin hotspots) and longitudinal filaments (actin trails) that are present inside the axon (cross-sections, bottom middle panels). Scale bars: 2 μm; 0.5 μm for cross-sections. Adapted from Ganguly et al. (2015).

Spines, the micron-size, mushroom-shaped extensions that bear excitatory synapses along dendrites in several neuron types, have been extensively imaged and studied over the years (Sala and Segal, 2014). The 1896 drawings from Cajal show Purkinje cell dendrites studded with spines (Fig. 10*A*, from García-López et al., 2007). EM visualized spines in brain sections, but imaging their actin content required specific filament labeling using myosin head decoration (Fig. 10*B*, from Markham and Fifková,

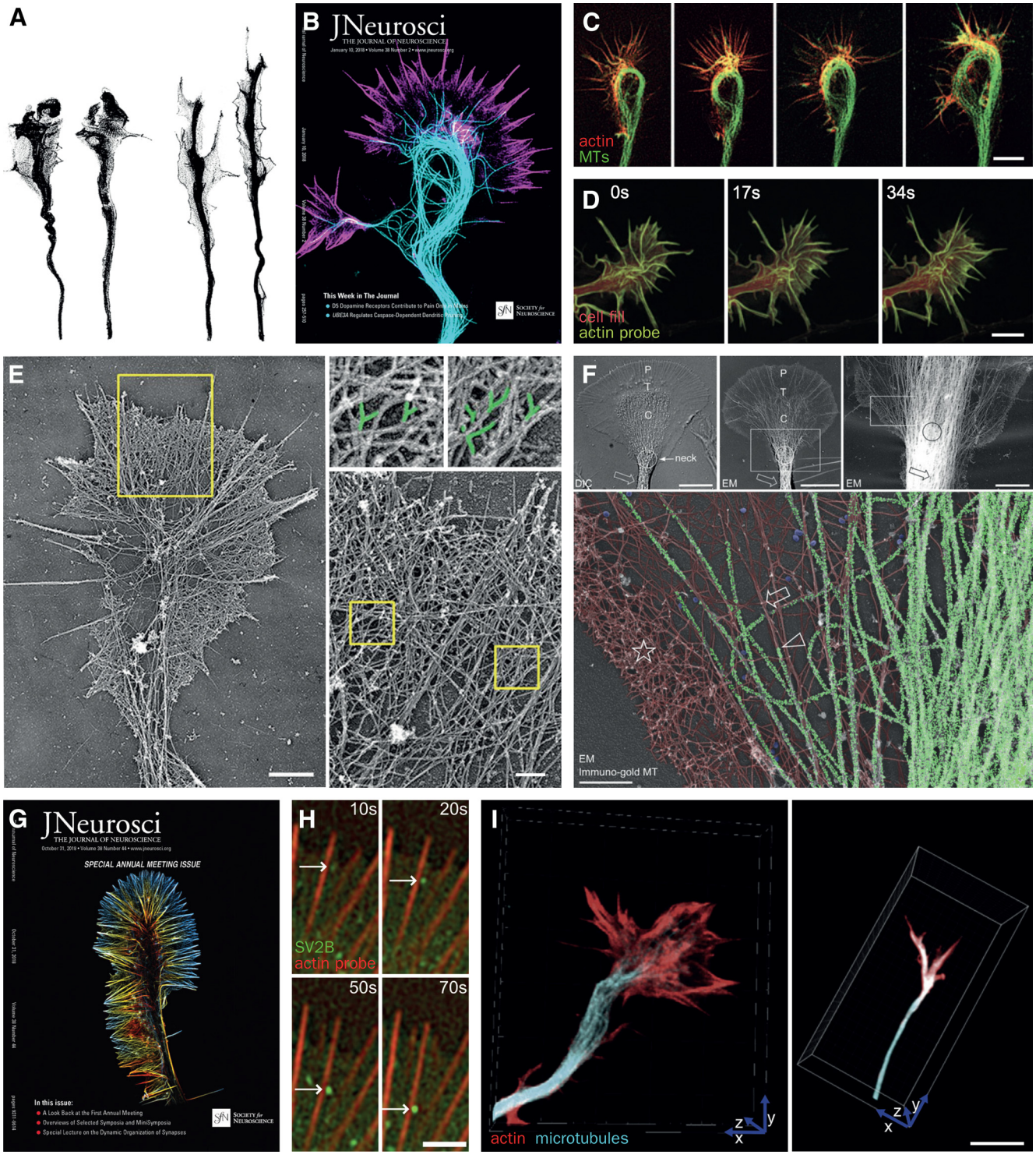

Figure 9. The neuronal growth cone cytoskeleton. ***A***, Growth cones from the spinal cord of E4 chick embryos stained with the Golgi method, as drawn by Cajal. Adapted from Cajal (1999). ***B***, Cover from the January 10, 2018 issue of the *Journal of Neuroscience* showing a STED image of a growth cone labeled for microtubules (cyan) and actin (magenta) (Biswas and Kalil, 2018). ***C***, Live-cell imaging of actin (injected phalloidin) and microtubules (injected tubulin) within the growth cone of a hamster cortical neuron in culture. Scale bar, 10 μm. Adapted from Dent and Kalil (2001). ***D***, Live growth cone of a rat hippocampal neuron expressing an actin probe (TdTomato-LifeAct, green) and a cytosolic marker (GFP, red), imaged by 3D-SIM. Scale bar, 2 μm. Adapted from Fiolka et al. (2012). ***E***, Platinum-replica EM of a growth cone from a differentiated B35 cell showing the actin meshwork with characteristic branches formed by Arp2/3-mediated nucleation (zoomed insets, green). Scale bars: Left, 1 μm; Right, 0.2 μm. Adapted from Korobova and Svitkina (2008). ***F***, Differential interference contrast (top left) and rotary-shadowed EM images of *Aplysia* bag neuron growth cones with the neck (circle) and central (C), transition (T), and peripheral (P) zones. Bottom, Immunogold-labeled microtubules (green) and actin filaments (red) forming a meshwork (star). An actin filament (arrow) connects to a microtubule tip (arrowhead). Scale bars: Top left and middle, 10 μm; Top right, 5 μm; Bottom, 1 μm. Adapted from Burnette et al. (2008). ***G***, Cover from the October 31, 2018 issue of the *Journal of Neuroscience* showing a Structured Illumination Microscopy (SIM) image of a growth cone labeled for actin, color-coded for depth (Igarashi et al., 2018). ***H***, Live-cell SIM showing trafficking of synaptic cargo SV2B (green) between actin-rich filopodia (red) at the growth cone of a differentiated NG108-15 cell. Scale bar, 2 μm. Adapted from Nozumi et al. (2017). ***I***, STED images of mouse hippocampal neuron growth cones in 2D (left) and 3D (right) collagen environments, labeled for tubulin (cyan) and actin (red). Scale bar, 5 μm. Adapted from Santos et al. (2020).

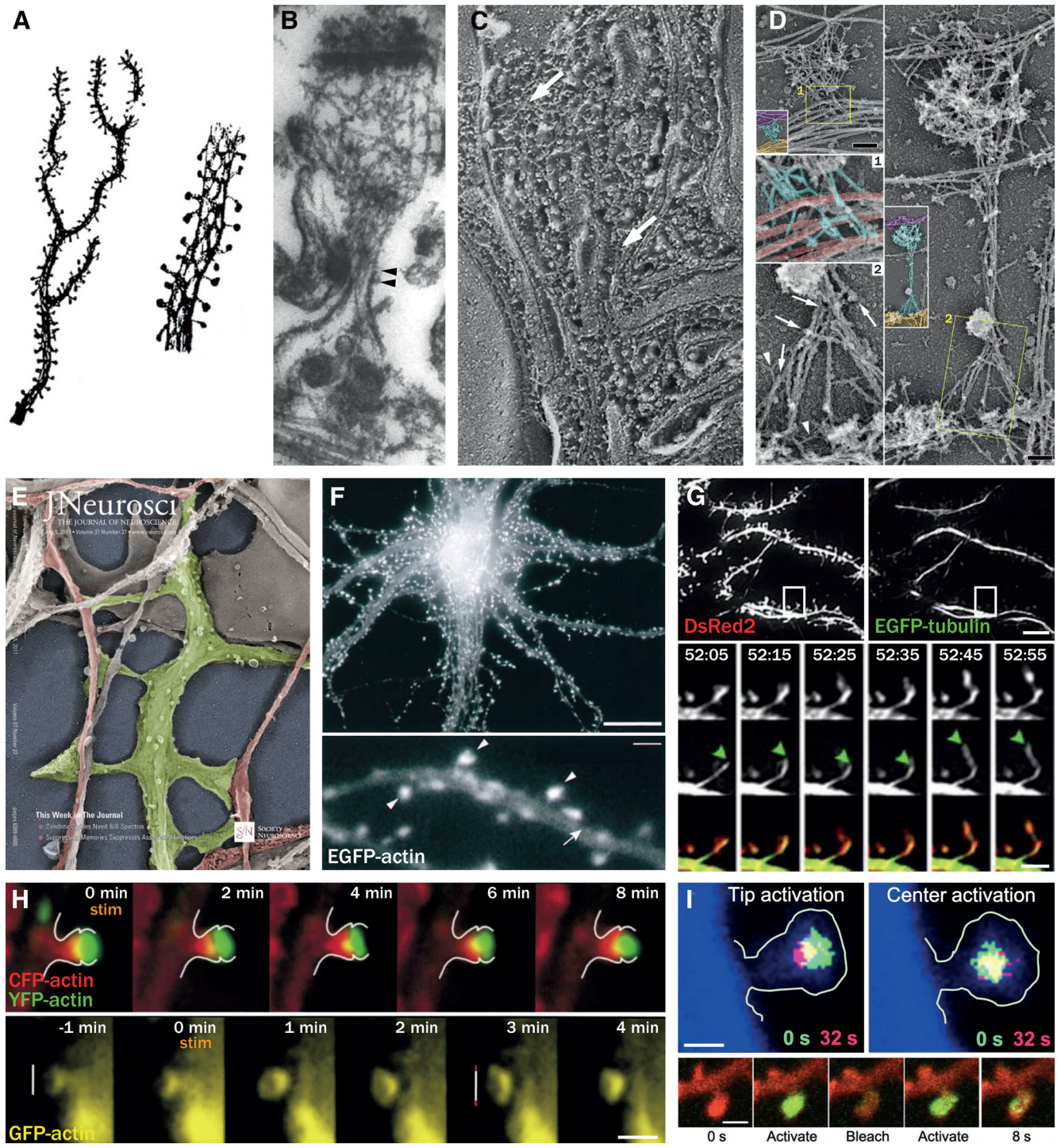

Figure 10. The dendritic spines, where the cytoskeleton drives synaptic plasticity. ***A***, Spines of a Purkinje cell stained with methylene blue, as drawn by Cajal. Adapted from García-López et al. (2007). ***B***, Thin-section EM of a dendritic spine with actin filaments labeled with myosin head; note the longitudinal filaments along the spine neck (arrowheads) and branched meshwork near the postsynapses. Adapted from Markham and Fifková (1986). ***C***, Cryo-fixed, cross-fractured dendritic spine of a mouse Purkinje cell showing a mesh of 6-10 nm filaments (arrows). Adapted from Landis and Reese (1983). ***D***, Platinum-replica EM of dendritic spines from cultured rat hippocampal neurons showing the longitudinal actin filaments along the neck and dense meshwork within the head. Scale bar, 0.2 μm. Adapted from Korobova and Svitkina (2010). ***E***, Cover from the July 5, 2017 issue of the *Journal of Neuroscience* showing a colored platinum replica EM image of a dendrite (green) contacting axons (red) in a neuronal culture (Efimova et al., 2017). ***F***, Live-cell imaging of actin-GFP in a mature hippocampal neuron in culture, showing actin concentration within dendritic spines (bottom, arrows). Scale bars: Top, 10 μm; Bottom, 2 μm. Adapted from Fischer et al. (1998). ***G***, Long-term Total Internal Reflection Fluorescence (TIRF) live-cell imaging of hippocampal neurons expressing a volume marker (DsRed2, top left, red on bottom overlay) and EGFP-tubulin (top right, green on bottom overlay). The bottom frames capture an event of microtubule invasion into a dendritic spine (green arrow). Scale bars: Top panels, 5 μm; Bottom frames, 2 μm. Adapted from Hu et al. (2008). ***H***, Top row, Morphologic plasticity of a dendritic spine of a neuron expressing CFP-actin in contact with an axon expressing YFP-actin, after photo-stimulation. Bottom row, Enlargement of a dendritic spine expressing GFP-actin (yellow) after photo-stimulation. Scale bar, 1 μm. Adapted from Colicos et al. (2001). ***I***, Top, Dendritic spines (labeled with TdTomato, blue) expressing photoactivable GFP (paGFP) just after (green) and 32 s after (red) activation. Tip activation shows an inward movement of actin. Bottom, Sequential activation/bleach/activation reveals the movement of newly polymerized actin within dendritic spines. Scale bars, 0.5 μm. Adapted from Frost et al. (2010).

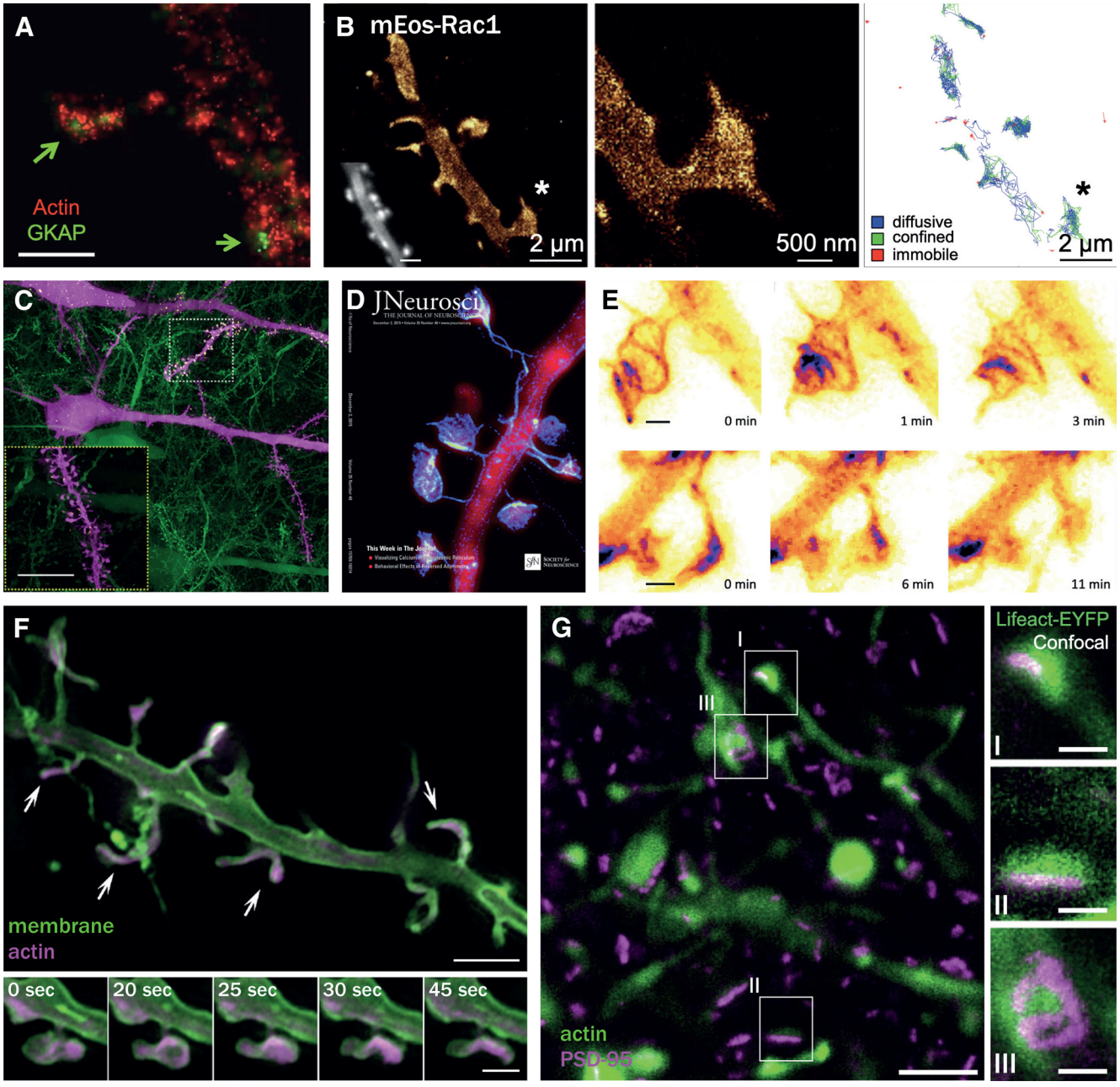

Figure 11. Super-resolved imaging of the dendritic spine cytoskeleton. ***A***, Early two-color PhotoActivated Localization Microscopy (PALM) image of actin-TdEos (red) and synaptic marker GKAP-Dronpa (green) in a dendritic spine. Scale bar, 1 μm. Adapted from Frost et al. (2010). ***B***, Localization images (left, with spine zoomed on middle) and three categories of trajectories (right) of single photoactivable actin regulator mEos-Rac1 in hippocampal neurons obtained by single particle tracking (spt) PALM. Adapted from Chazeau et al. (2014). ***C***, The combination of expansion microscopy and lattice-light sheet imaging can resolve individual spines and synapses of Thy1-GFP-labeled mouse neurons in the visual cortex within a volume of expanded brain. Scale bars: 50 μm; Inset, 10 μm. Adapted from Guo et al. (2019). ***D***, Cover from the December 2, 2015 issue of the *Journal of Neuroscience* showing a STED image of dendritic spines from a rat hippocampal neuron labeled with an actin probe (LifeAct-Venus, blue) and a volume marker (mCherry, red) (Chevy et al., 2015). ***E***, Live STED images of the actin probe LifeAct-YFP expressed in an organotypic slice culture showing the rearrangement of actin and change of the spine shape over minutes. Scale bars, 0.5 μm. Adapted from Urban et al. (2011). ***F***, Live grazing-incidence SIM image of a cultured hippocampal neuron expressing a membrane marker (memGFP) and an actin probe (LifeAct-mCherry) concentrated in spines (arrows), after chemical stimulation with glycine that induces morphologic plasticity. Scale bars: Top, 2 μm; Bottom frames, 1 μm. Adapted from Guo et al. (2018). ***G***, *In vivo* imaging of postsynaptic densities in the cortex from a living Halo-PSD95 transgenic mouse treated with SiR-Halo ligand (magenta) and infected with LifeAct-YFP (green), which labels dendritic spines. Scale bars: Left, 2 μm; Right, 0.5 μm. Adapted from Masch et al. (2018).

1986). Platinum replica EM, either of deep-etched tissue (Fig. 10*C*, from Landis and Reese, 1983) or fixed cultures (Fig. 10*D*, from Korobova and Svitkina, 2010), highlights the dense meshwork of actin around the postsynaptic density, as well as the longitudinal filaments along the thin spine neck. Nonextracted samples with intact plasma membrane show how spines and axons contact to form synapses (Fig. 10*E*, from Efimova et al., 2017). Fluorescent imaging using fluorescent protein-tagged actin probes are used to image spines in living neurons (Fig. 10*F*, from Fischer et al., 1998), and long-term imaging revealed the rare event of microtubules transiently invading spines, a key event for activity-dependent postsynaptic remodeling (Fig. 10*G*,

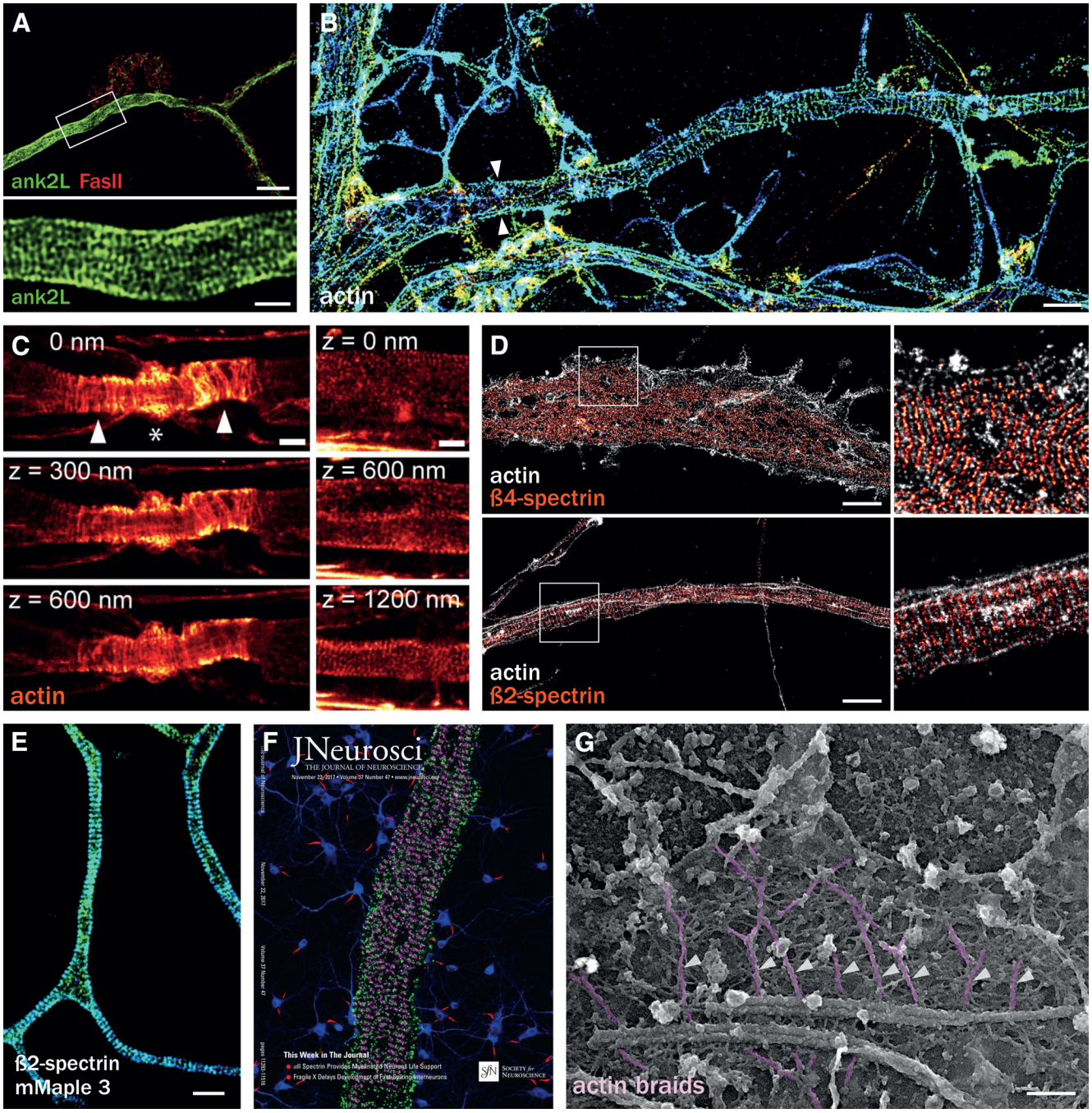

Figure 12. The submembrane periodic actin/spectrin scaffold along axons. ***A***, Early published observation of a 200 nm periodic scaffold along axons near neuromuscular junctions (FasII labeling, red), as revealed by labeling the *Drosophila* ankyrin ank2L (green) and imaged by SIM. Scale bars: Top, 5 μm; Bottom, 1 μm. Adapted from Pielage et al. (2008). ***B***, Depth color-coded 3D-STORM image of actin along the axon (extending from the hillock, arrowheads) of a cultured hippocampal neuron, revealing regularly spaced actin rings every 190 nm. Scale bar, 1 μm. Adapted from Xu et al. (2013). ***C***, The periodic actin/spectrin scaffold is present along myelinated fibers, as shown by phalloidin labeling of mouse sciatic nerve imaged by STED. Scale bars, 1 μm. Adapted from D'Este et al. (2016). ***D***, Two-color DNA-PAINT of rat hippocampal neurons in culture shows that actin rings (gray) are spaced every 190 nm by spectrin tetramers containing β4-spectrin along the proximal axon (orange, top), and β2-spectrin along the distal axon (orange, bottom). Scale bars, 2 μm. Adapted from Vassilopoulos et al. (2019). ***E***, The periodic scaffold visualized in living cells using PALM of β2-spectrin-mMaple3 in cultured neurons. Scale bar, 1 μm. Adapted from Zhong et al. (2014). ***F***, Cover of the November 22, 2017 issue of the *Journal of Neuroscience* showing that spectrin tetramers along the axon initial segment are composed of α2-spectrin (green) and β4-spectrin (magenta) by 2-color DNA-PAINT (Huang et al., 2017). ***G***, Platinum-replica EM of unroofed cultured hippocampal neurons, showing the submembrane, 190 nm spaced actin braids made of long, intertwined actin filaments along the axon. Scale bar, 200 nm. Adapted from Vassilopoulos et al. (2019).

from Hu et al., 2008). Two-color imaging of CFP and YFP-actin in neurons cultured on silicon substrate highlighted how both the presynapse and postsynapse remodel after local photo-stimulation (Fig. 10*H*, from Colicos et al., 2001), and local photo-activation was used to probe actin polymerization dynamics within the spine head (Fig. 10*I*, from Frost et al., 2010).

The small size of spines, micron-size heads and necks that can be as thin as a few tens of nanometers, made them a target of choice for super-resolution imaging using a range of techniques (Robinson et al., 2016). Early super-resolved images of spine actin were obtained by PALM (Fig. 11*A*, from Frost et al., 2010), and the photo-activation principle behind PALM allowed the

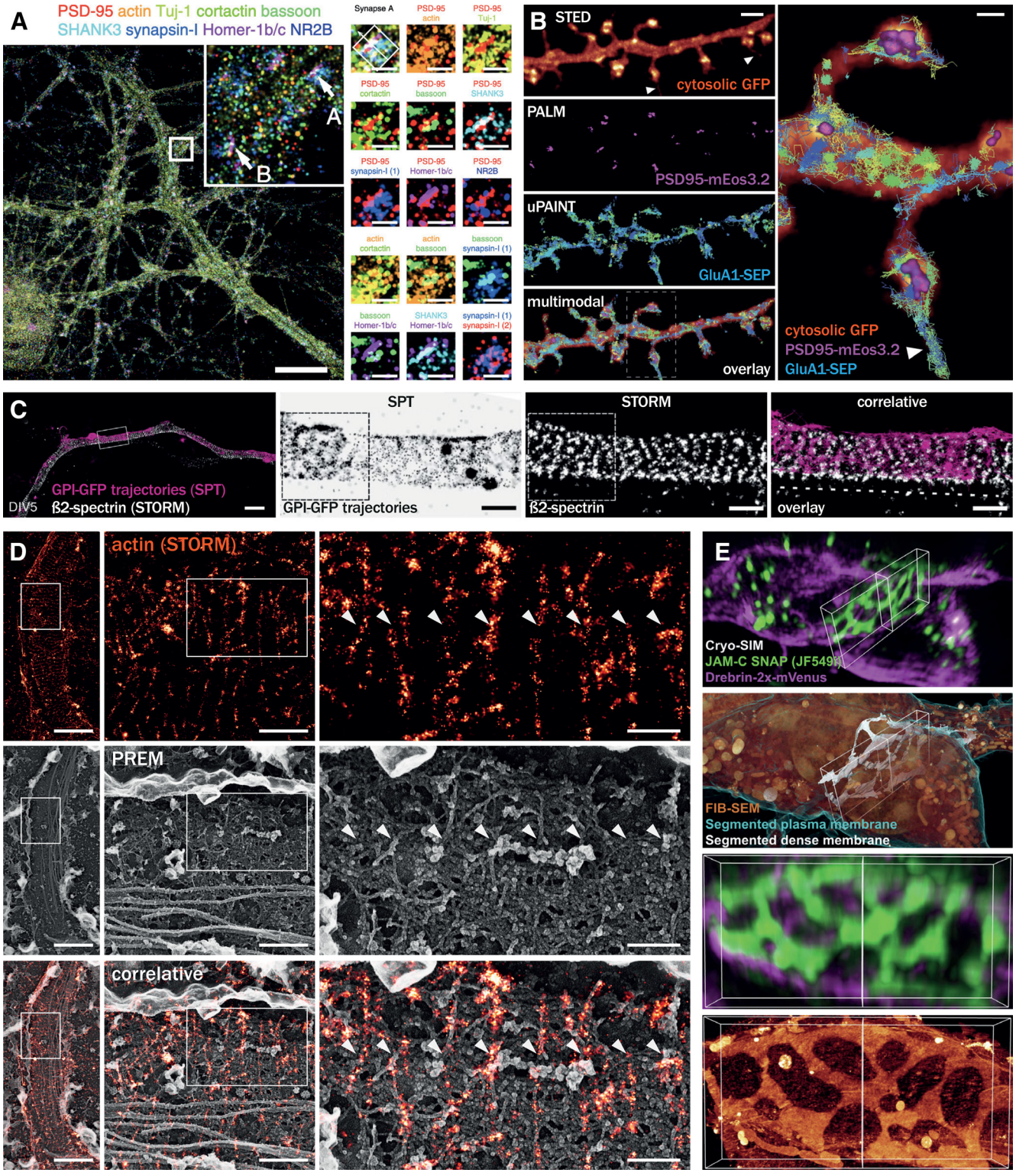

Figure 13. Multiplexed, multimodal, and correlative approaches. ***A***, DNA-PAINT allows multiplexed sequential imaging of 10 targets, including actin and tubulin, to reveal the nanoscale organization of synapses. Scale bars: Left, 10 μm; Right, insets, 0.5 μm. Adapted from Guo et al. (2019). ***B***, Multimodal STED/Single Molecule Localization Microscopy (SMLM) imaging of a living neuron; STED of a cytosolic marker (GFP, orange) visualizes neuronal morphology, while PALM of PSD95-mEos3.2 resolves synaptic nano-domains, and uPAINT tracking of GluA1-SEP determines the single-molecule mobility of glutamate receptors. Scale bars: Left, 2 μm; Right, inset, 0.5 μm. Adapted from Inavalli et al. (2019). ***C***, Correlative SPT of GPI-GFP (magenta) and STORM of β2-spectrin (gray) reveals that the diffusion of membrane proteins along the proximal axon is compartmented by the periodic submembrane scaffold. Scale bars: Left, 2 μm; Right, insets, 0.5 μm. Adapted from Albrecht et al. (2016). ***D***, Correlative STORM and platinum-replica EM demonstrate that actin rings seen by STORM are the actin braids seen by platinum-replica EM, combining molecular identification and ultrastructure. Scale bars: Left, 2 μm; Middle, 0.5 μm; Right, 200 nm. Adapted from Vassilopoulos et al. (2019). ***E***, Correlative imaging of cell-cell junctions in cryofixed cerebellar granule neurons: cryo-SIM (top) of the junctional protein JAM-C (green, revealed by SNAP-JF549i) and drebrin-2×-mVenus (magenta) combined with focused ion beam milling/scanning EM (second panel, with segmented plasma membrane in cyan, intracellular components in orange, and cell-cell junction in gray). Bottom panels, Zooms on the cell-cell junction area. White box dimensions are 9.7 μm × 4.7 μm × 1.1 μm. Adapted from Hoffman et al. (2020).

mobility of individual actin-binding proteins to be tracked within spines, using a technique called sptPALM; this revealed distinct localization and mechanisms of actin nucleation (Fig. 11*B*, from Chazeau et al., 2014). Expansion microscopy coupled to fast, large-volume lattice light-sheet microscopy recently provided stunning images of whole cortical volumes with thousands of identified spines and their associated synapses (Fig. 11*C*, from Gao et al., 2019). STED microscopy can visualize the reticulated architecture of actin within spines using probes such as fluorescent LifeAct in cultures (Fig. 11*D*, from Chevy et al., 2015) and in organotypic slices (Fig. 11*E*, from Urban et al., 2011). SIM has also been used to image the activity-dependent structural plasticity at spines (Fig. 11*F*, from Guo et al., 2018). Finally, super-resolution imaging of spines and their associated synapses is now possible directly in the cortex of living animals, using transgenic mice and/or viral transduction of probes (Fig. 11*G*, from Masch et al., 2018).

While super-resolution microscopy refined our knowledge of known structures, such as growth cones and dendritic spines, it also revealed a completely new cytoskeletal organization in axons (Leterrier et al., 2017). An early SIM observation in *Drosophila* had reported that ankyrin, a submembrane scaffold protein, formed patterns along the axon shaft with a ~200 nm regularity (Fig. 12*A*, from Pielage et al., 2008). In 2013, optimized STORM in cultured neurons and organotypic slices revealed that actin forms circumferential rings, regularly spaced every 190 nm along axons (Fig. 12*B*, from Xu et al., 2013). Actin rings are found along all axons, including myelinated ones (Fig. 12*C*, from D'Este et al., 2016), in a variety of neuronal types and organisms (Papandréou and Leterrier, 2018). The 190 nm distance corresponds to the length of spectrin tetramers that connect adjacent rings, forming a periodic submembrane scaffold that appears as alternating bands of spectrin and actin on 2-color SMLM images (Fig. 12*D*, from Vassilopoulos et al., 2019). Spectrin periodicity has been observed along the axon of living neurons using PALM of photo-activable β2-spectrin (Fig. 12*E*, from Zhong et al., 2014). Spectrin tetramers are composed of two α and two β subunits, with α2-spectrin associating with β4-spectrin in the initial segment (Fig. 12*F*, from Huang et al., 2017), whereas tetramers are made of α2- and β2-spectrin along the distal axon (Fig. 12*D*). Finally, platinum replica EM after unroofing (mechanical removal of the dorsal part of the cell) (Mazia et al., 1975) was recently able to visualize rings as regularly spaced actin "braids" connected by a submembrane spectrin mesh in unroofed axons of cultured neurons (Fig. 12*G*, from Vassilopoulos et al., 2019).

Looking back at images of the neuronal cytoskeleton from the beautiful drawings of the 19th century to the fantastically detailed electron and optical microscopy techniques of our time, one can only be excited about the next steps in this journey. Beyond faster, gentler, higher-resolution imaging, one direction that is poised to bring new crucial insights is the capacity to image multiple targets using multiplexed, multimodal and correlative approaches. Techniques, such as DNA-PAINT, where fluorescent labels are transiently attached to DNA-coupled probes, can now sequentially image $\geq$10 proteins, allowing high-content mapping of the neuronal architecture (Fig. 13*A*, from Guo et al., 2019). Multiple super-resolution techniques, such as STED, STORM, and single-particle tracking, can be combined to reveal the dynamic interplay that underlies synaptic physiology (Fig. 13*B*, from Inavalli et al., 2019) or the role of the periodic submembrane scaffold in the diffusion of axonal membrane proteins (Fig. 13*C*, from Albrecht et al., 2016). Correlative super-resolution imaging and EM demonstrated that the actin braids visualized by platinum replica EM along the periodic scaffold were indeed the actin rings imaged by STORM (Fig. 13*D*, from Vassilopoulos et al., 2019), and visualized the three-dimensional details of cell-cell contacts in granule cells by superimposing the molecular specificity of SIM with the ultrastructure context from focused ion beam milling/scanning EM (Fig. 13*E*, from Hoffman et al., 2020). Advances in engineering and instrumentation, as well as the ever-growing capabilities for data processing, quantification, and analysis, will undoubtedly revolutionize our understanding of the neuronal cytoskeleton in the years to come. But fundamentally, the key to new discoveries will remain the eye of the experimenter, be it literal or metaphorical: the talent of scientists throughout the years to extract meaningful information and knowledge from the fascinating images of shimmering butterflies.

References

Albrecht D, Winterflood CM, Sadeghi M, Tschager T, Noé F, Ewers H (2016) Nanoscopic compartmentalization of membrane protein motion at the axon initial segment. J Cell Biol 215:37–46.

Allison DW, Chervin AS, Gelfand VI, Craig AM (2000) Postsynaptic scaffolds of excitatory and inhibitory synapses in hippocampal neurons: maintenance of core components independent of actin filaments and microtubules. J Neurosci 20:4545–4554.

Atherton J, Stouffer M, Francis F, Moores CA (2018) Microtubule architecture in vitro and in cells revealed by cryo-electron tomography. Acta Crystallogr D Struct Biol 74:572–584.

Baas PW, Lin S (2011) Hooks and comets: the story of microtubule polarity orientation in the neuron. Dev Neurobiol 71:403–418.

Baas PW, Deitch JS, Black MM, Banker GA (1988) Polarity orientation of microtubules in hippocampal neurons: uniformity in the axon and nonuniformity in the dendrite. Proc Natl Acad Sci USA 85:8335–8339.

Baas PW, Ahmad FJ, Pienkowski TP, Brown A, Black MM (1993) Sites of microtubule stabilization for the axon. J Neurosci 13:2177–2185.

Bartlett WP, Banker GA (1984) An electron microscopic study of the development of axons and dendrites by hippocampal neurons in culture: I. Cells which develop without intercellular contacts. J Neurosci 4:1944–1953.

Biswas S, Kalil K (2018) The microtubule-associated protein tau mediates the organization of microtubules and their dynamic exploration of actin-rich lamellipodia and filopodia of cortical growth cones. J Neurosci 38:291–307.

Bray D, Bunge MB (1981) Serial analysis of microtubules in cultured rat sensory axons. J Neurocytol 10:589–605.

Burnette DT, Ji L, Schaefer AW, Medeiros NA, Danuser G, Forscher P (2008) Myosin II activity facilitates microtubule bundling in the neuronal growth cone neck. Dev Cell 15:163–169.

Cáceres A, Banker GA, Binder L (1986) Immunocytochemical localization of tubulin and microtubule-associated protein 2 during the development of hippocampal neurons in culture. J Neurosci 6:714–722.

Cajal S (1999) Histogenesis of the spinal cord and spinal ganglia. In: Texture of the nervous system of man and the vertebrates, pp 517–584. Vienna: Springer.

Chabrier R, Janke C (2017) The comeback of hand drawing in modern life sciences. Nat Rev Mol Cell Bio 150:137–138.

Chalfie M, Thomson JN (1982) Structural and functional diversity in the neuronal microtubules of *Caenorhabditis elegans*. J Cell Biol 93:15–23.

Chan-Palay V (1972) The tripartite structure of the undercoat in initial segments of Purkinje cell axons. Z Anat Entwicklungsgesch 139:1–10.

Charrier C, Ehrensperger MV, Dahan M, Lévi S, Triller A (2006) Cytoskeleton regulation of glycine receptor number at synapses and diffusion in the plasma membrane. J Neurosci 26:8502–8511.

Chazeau A, Mehidi A, Nair D, Gautier JJ, Leduc C, Chamma I, Kage F, Kechkar A, Thoumine O, Rottner K, Choquet D, Gautreau A, Sibarita JB, Giannone G (2014) Nanoscale segregation of actin nucleation and elongation factors determines dendritic spine protrusion. EMBO J 33:2745–2764.

Cheng TP, Reese TS (1988) Compartmentalization of anterogradely and retrogradely transported organelles in axons and growth cones from chick optic tectum. J Neurosci 8:3190–3199.

Chevy Q, Heubl M, Goutierre M, Backer S, Moutkine I, Eugène E, Bloch-Gallego E, Lévi S, Poncer JC (2015) KCC2 gates activity-driven AMPA receptor traffic through cofilin phosphorylation. J Neurosci 35:15772–15786.

Colicos MA, Collins BE, Sailor MJ, Goda Y (2001) Remodeling of synaptic actin induced by photoconductive stimulation. Cell 107:605–616.

Coons AH, Creech HJ, Jones RN, Berliner E (1942) The demonstration of pneumococcal antigen in tissues by the use of fluorescent antibody. J Immunol 45:159.

Dailey M, Bridgman P (1989) Dynamics of the endoplasmic reticulum and other membranous organelles in growth cones of cultured neurons. J Neurosci 9:1897–1909.

Dent EW, Kalil K (2001) Axon branching requires interactions between dynamic microtubules and actin filaments. J Neurosci 21:9757–9769.

D'Este E, Kamin D, Velte C, Göttfert F, Simons M, Hell SW (2016) Subcortical cytoskeleton periodicity throughout the nervous system. Sci Rep 6:22741.

Efimova N, Korobova F, Stankewich MC, Moberly AH, Stolz DB, Wang J, Kashina A, Ma M, Svitkina T (2017) βIII spectrin is necessary for formation of the constricted neck of dendritic spines and regulation of synaptic activity in neurons. J Neurosci 37:6442–6459.

Fiolka R, Shao L, Rego EH, Davidson MW, Gustafsson MG (2012) Time-lapse two-color 3D imaging of live cells with doubled resolution using structured illumination. Proc Natl Acad Sci USA 109:5311–5315.

Fischer M, Kaech S, Knutti D, Matus A (1998) Rapid actin-based plasticity in dendritic spines. Neuron 20:847–854.

Frixione E (2009) Cajal's second great battle for the neuron doctrine: the nature and function of neurofibrils. Brain Res Rev 59:393–409.

Frost NA, Shroff H, Kong H, Betzig E, Blanpied TA (2010) Single-molecule discrimination of discrete perisynaptic and distributed sites of actin filament assembly within dendritic spines. Neuron 67:86–99.

Gallo G, Letourneau PC (1998) Localized sources of neurotrophins initiate axon collateral sprouting. J Neurosci 18:5403–5414.

Ganguly A, Tang Y, Wang L, Ladt K, Loi J, Dargent B, Leterrier C, Roy S (2015) A dynamic formin-dependent deep F-actin network in axons. J Cell Biol 210:401–417.

Gao R, Asano SM, Upadhyayula S, Pisarev I, Milkie DE, Liu TL, Singh V, Graves A, Huynh GH, Zhao Y, Bogovic J, Colonell J, Ott CM, Zugates C, Tappan S, Rodriguez A, Mosaliganti KR, Sheu SH, Pasolli HA, Pang S, et al. (2019) Cortical column and whole-brain imaging with molecular contrast and nanoscale resolution. Science 363:eaau8302.

García-López P, García-Marín V, Freire M (2007) The discovery of dendritic spines by Cajal in 1888 and its relevance in the present neuroscience. Prog Neurobiol 83:110–130.

Gonatas NK, Robbins E (1965) The homology of spindle tubules and neurotubules in the chick embryo retina. Protoplasma 59:377–391.

Gray EG, Guillery RW (1966) Synaptic morphology in the normal and degenerating nervous system. Int Rev Cytol 19:111–182.

Groc L, Choquet D (2020) Linking glutamate receptor movements and synapse function. Science 368:eaay4631.

Guo SM, Veneziano R, Gordonov S, Li L, Danielson E, Arce KP, de Park D, Kulesa AB, Wamhoff EC, Blainey PC, Boyden ES, Cottrell JR, Bathe M (2019) Multiplexed and high-throughput neuronal fluorescence imaging with diffusible probes. Nat Commun 10:4377.

Guo Y, Li D, Zhang S, Yang Y, Liu JJ, Wang X, Liu C, Milkie DE, Moore RP, Tulu US, Kiehart DP, Hu J, Lippincott-Schwartz J, Betzig E, Li D (2018) Visualizing intracellular organelle and cytoskeletal interactions at nanoscale resolution on millisecond timescales. Cell 175:1430–1442.e17.

Heuser JE (2011) The origins and evolution of freeze-etch electron microscopy. J Electron Microsc (Tokyo) 60 Suppl 1:S3–S29.

Hirokawa N (1982) Cross-linker system between neurofilaments, microtubules and membranous organelles in frog axons revealed by the quick-freeze, deep-etching method. J Cell Biol 94:129–142.

Hoffman DP, Shtengel G, Xu CS, Campbell KR, Freeman M, Wang L, Milkie DE, Pasolli HA, Iyer N, Bogovic JA, Stabley DR, Shirinifard A, Pang S, Peale D, Schaefer K, Pomp W, Chang CL, Lippincott-Schwartz J, Kirchhausen T, Solecki DJ, et al. (2020) Correlative three-dimensional super-resolution and block-face electron microscopy of whole vitreously frozen cells. Science 367:eaaz5357.

Horridge GA, Mackay B (1962) Naked axons and symmetrical synapses in coelenterates. J Cell Sci s3-103:531–541.

Hu X, Viesselmann C, Nam S, Merriam E, Dent EW (2008) Activity-dependent dynamic microtubule invasion of dendritic spines. J Neurosci 28:13094–13105.

Huang CY, Zhang C, Ho TS, Oses-Prieto J, Burlingame AL, Lalonde J, Noebels JL, Leterrier C, Rasband MN (2017) αII spectrin forms a periodic cytoskeleton at the axon initial segment and is required for nervous system function. J Neurosci 37:11311–11322.

Igarashi M, Nozumi M, Wu LG, Zanacchi FC, Katona I, Barna L, Xu P, Zhang M, Xue F, Boyden E (2018) New observations in neuroscience using superresolution microscopy. J Neurosci 38:9459–9467.

Inavalli VV, Lenz MO, Butler C, Angibaud J, Compans B, Levet F, Tønnesen J, Rossier O, Giannone G, Thoumine O, Hosy E, Choquet D, Sibarita JB, Nägerl UV (2019) A super-resolution platform for correlative live single-molecule imaging and STED microscopy. Nat Methods 16:1263–1268.

Jacquemet G, Carisey AF, Hamidi H, Henriques R, Leterrier C (2020) The cell biologist's guide to super-resolution microscopy. J Cell Sci 133: jcs240713.

Jurriens D, Batenburg V, Katrukha EA, Kapitein LC (2020) Mapping the neuronal cytoskeleton using expansion microscopy. In: Methods in Cell Biology. Academic Press.

Kapitein LC, Hoogenraad CC (2015) Building the neuronal microtubule cytoskeleton. Neuron 87:492–506.

Katanov C, Novak N, Vainshtein A, Golani O, Dupree JL, Peles E (2020) N-Wasp regulates oligodendrocyte myelination. J Neurosci. Advance online publication. Retrieved Jun 29, 2020. doi: 10.1523/JNEUROSCI.0912-20.2020.

Korobova F, Svitkina T (2008) Arp2/3 complex is important for filopodia formation, growth cone motility, and neuritogenesis in neuronal cells. Mol Biol Cell 19:1561–1574.

Korobova F, Svitkina T (2010) Molecular architecture of synaptic actin cytoskeleton in hippocampal neurons reveals a mechanism of dendritic spine morphogenesis. Mol Biol Cell 21:165–176.

Krstić RV (1979) Ultrastructure of the mammalian cell: an atlas. London: Springer.

Kuczmarski ER, Rosenbaum JL (1979) Studies on the organization and localization of actin and myosin in neurons. J Cell Biol 80:356–371.

Kusumi A, Nakada C, Ritchie K, Murase K, Suzuki K, Murakoshi H, Kasai RS, Kondo J, Fujiwara T (2005) Paradigm shift of the plasma membrane concept from the two-dimensional continuum fluid to the partitioned fluid: high-speed single-molecule tracking of membrane molecules. Annu Rev Biophys Biomol Struct 34:351–378.

Landis DM, Reese TS (1983) Cytoplasmic organization in cerebellar dendritic spines. J Cell Biol 97:1169–1178.

Leterrier C, Dubey P, Roy S (2017) The nano-architecture of the axonal cytoskeleton. Nat Rev Neurosci 18:713–726.

Letourneau PC (1982) Analysis of microtubule number and length in cytoskeletons of cultured chick sensory neurons. J Neurosci 2:806–814.

Marchisio PC, Osborn M, Weber K (1978) The intracellular organization of actin and tubulin in cultured C-1300 mouse neuroblastoma cells (clone NB41A3). J Neurocytol 7:571–582.

Markham JA, Fifková E (1986) Actin filament organization within dendrites and dendritic spines during development. Dev Brain Res 27:263–269.

Masch JM, Steffens H, Fischer J, Engelhardt J, Hubrich J, Keller-Findeisen J, D'Este E, Urban NT, Grant SG, Sahl SJ, Kamin D, Hell SW (2018) Robust nanoscopy of a synaptic protein in living mice by organic-fluorophore labeling. Proc Natl Acad Sci USA 115:E8047–E8056.

Mazia D, Schatten G, Sale W (1975) Adhesion of cells to surfaces coated with polylysine: applications to electron microscopy. J Cell Biol 66:198–200.

McCormick LE, Gupton SL (2020) Mechanistic advances in axon pathfinding. Curr Opin Cell Biol 63:11–19.

Meller K (1987) The cytoskeleton of cryofixed Purkinje cells of the chicken cerebellum. Cell Tissue Res 247:155–165.

Mikhaylova M, Cloin BM, Finan K, van den Berg R, Teeuw J, Kijanka MM, Sokolowski M, Katrukha EA, Maidorn M, Opazo F, Moutel S, Vantard M, Perez F, van Bergen en Henegouwen PM, Hoogenraad CC, Ewers H, Kapitein LC (2015) Resolving bundled microtubules using anti-tubulin nanobodies. Nat Commun 6:7933.

Nakada C, Ritchie K, Oba Y, Nakamura M, Hotta Y, Iino R, Kasai RS, Yamaguchi K, Fujiwara T, Kusumi A (2003) Accumulation of anchored

proteins forms membrane diffusion barriers during neuronal polarization. Nat Cell Biol 5:626–632.
Nozumi M, Nakatsu F, Katoh K, Igarashi M (2017) Coordinated movement of vesicles and actin bundles during nerve growth revealed by superresolution microscopy. Cell Rep 18:2203–2216.
Papandréou MJ, Leterrier C (2018) The functional architecture of axonal actin. Mol Cell Neurosci 91:151–159.
Pielage J, Cheng L, Fetter RD, Carlton PM, Sedat JW, Davis GW (2008) A presynaptic giant ankyrin stabilizes the NMJ through regulation of presynaptic microtubules and transsynaptic cell adhesion. Neuron 58:195–209.
Prokop A (2020) Cytoskeletal organization of axons in vertebrates and invertebrates. J Cell Biol 219 Available at: http://dx.doi.org/10.1083/jcb.201912081.
Robinson CM, Patel MR, Webb DJ (2016) Super resolution microscopy is poised to reveal new insights into the formation and maturation of dendritic spines. F1000Res 5:1468.
Ruthel G, Hollenbeck PJ (2003) Response of mitochondrial traffic to axon determination and differential branch growth. J Neurosci 23:8618–8624.
Sabatini DD, Bensch K, Barrnett RJ (1963) Cytochemistry and electron microscopy: the preservation of cellular ultrastructure and enzymatic activity by aldehyde fixation. J Cell Biol 17:19–58.
Sala C, Segal M (2014) Dendritic spines: the locus of structural and functional plasticity. Physiol Rev 94:141–188.
Sandborn E, Koen PF, McNabb JD, Moore G (1964) Cytoplasmic microtubules in mammalian cells. J Ultra Mol Struct 11:123–138.
Santos TE, Schaffran B, Broguière N, Meyn L, Zenobi-Wong M, Bradke F (2020) Axon growth of CNS neurons in three dimensions is amoeboid and independent of adhesions. Cell Rep 32:107907.
Schnapp BJ, Reese TS (1982) Cytoplasmic structure in rapid-frozen axons. J Cell Biol 94:667–669.
Slaughter T, Wang J, Black MM (1997) Microtubule transport from the cell body into the axons of growing neurons. J Neurosci 17:5807–5819.
Smith DS (1971) On the significance of cross-bridges between microtubules and synaptic vesicles. Philos Trans R Soc Lond B Biol Sci 261:395–405.
Smith DS, Järlfors U, Beránek R (1970) The organization of synaptic axoplasm in the lamprey (*Petromyzon marinus*) central nervous system. J Cell Biol 46:199–219.
Stepanova T, Slemmer J, Hoogenraad CC, Lansbergen G, Dortland B, Zeeuw CI, Grosveld F, van Cappellen G, Akhmanova A, Galjart N (2003) Visualization of microtubule growth in cultured neurons via the use of EB3-GFP (end-binding protein 3-green fluorescent protein). J Neurosci 23:2655–2664.
Stern S, Debre E, Stritt C, Berger J, Posern G, Knöll B (2009) A nuclear actin function regulates neuronal motility by serum response factor-dependent gene transcription. J Neurosci 29:4512–4518.
Tas RP, Kapitein LC (2018) Exploring cytoskeletal diversity in neurons. Science 361:231–232.
Tas RP, Chazeau A, Cloin BM, Lambers ML, Hoogenraad CC, Kapitein LC (2017) Differentiation between oppositely oriented microtubules controls polarized neuronal transport. Neuron 96:1264–1271.e5.
Urban NT, Willig KI, Hell SW, Nagerl UV (2011) STED nanoscopy of actin dynamics in synapses deep inside living brain slices. Biophys J 101:1277–1284.
van Bommel B, Konietzny A, Kobler O, Bär J, Mikhaylova M (2019) F-actin patches associated with glutamatergic synapses control positioning of dendritic lysosomes. EMBO J 38:e101183.
Vassilopoulos S, Gibaud S, Jimenez A, Caillol G, Leterrier C (2019) Ultrastructure of the axonal periodic scaffold reveals a braid-like organization of actin rings. Nat Commun 10:5803.
Xu K, Zhong G, Zhuang X (2013) Actin, spectrin, and associated proteins form a periodic cytoskeletal structure in axons. Science 339:452–456.
Yamada KM, Spooner BS, Wessells NK (1970) Axon growth: roles of microfilaments and microtubules. Proc Natl Acad Sci USA 66:1206–1212.
Yau KW, Schätzle P, Tortosa E, Pagès S, Holtmaat A, Kapitein LC, Hoogenraad CC (2016) Dendrites in vitro and in vivo contain microtubules of opposite polarity and axon formation correlates with uniform plus-end-out microtubule orientation. J Neurosci 36:1071–1085.
Yu W, Baas PW (1994) Changes in microtubule number and length during axon differentiation. J Neurosci 14:2818–2829.
Zhong G, He J, Zhou R, Lorenzo D, Babcock HP, Bennett V, Zhuang X (2014) Developmental mechanism of the periodic membrane skeleton in axons. Elife 3:e04581.
Zwirn S (2015) Butterflies of the soul: Cajal's neuron theory and art. J Aesthetic Educ 49:105–119.